

Entangled Cavity State Generation through Engineered Dissipation

Mikhail Mamaev
Department of Physics
McGill University, Montreal
August 2017

A thesis submitted to McGill University in partial fulfillment of the
requirements of the degree of M.Sc.

© Mikhail Mamaev 2017

Contents

Abstract	ii
Résumé	iii
Acknowledgments	iv
1 Introduction	1
2 Relevant background from quantum optics	3
2.1 Commonly-used states	3
2.1.1 Coherent states	3
2.1.2 Squeezed-states	4
2.1.3 Cat states	6
2.1.4 Wigner function	8
2.2 Lindblad master equation	9
2.2.1 Equation form	9
2.2.2 Superoperator formalism	11
2.3 Cascaded systems	13
2.3.1 Overview	13
2.3.2 Master equation	14
2.3.3 Synthetic implementations	16
2.4 Perfect absorber recipe	17
3 Two-mode squeezing via broken time-reversal symmetry	20
3.1 Perfect absorber recipe	22
3.2 Squeezed-state properties	26
3.2.1 Cavity mode basis and two-mode squeezing	26
3.2.2 Covariance matrix	27
3.2.3 Parametric instability	28
3.2.4 Logarithmic negativity	29
3.3 Adiabatic continuity	30
3.4 Intrinsic loss	33
3.5 Conclusion	34

4	Entangled cat state stabilization	36
4.1	Single Kerr parametric oscillator	38
4.1.1	Hamiltonian and eigenstates	39
4.1.2	Damping and degenerate perturbation theory	40
4.1.3	Slow rates	43
4.2	Two-cavity Kerr perfect absorber	47
4.3	Cat state properties	50
4.4	Steady-state in cavity mode basis	52
4.5	Alternate detuning implementation	55
4.6	System imperfections	58
4.6.1	Slow rates	58
4.6.2	Intrinsic loss	59
4.6.3	Parameter mismatch	61
4.7	Conclusion	62
5	Adiabatic ramping	63
5.1	Stabilization speedup	64
5.2	Metastable entangled-cat generation	65
6	Conclusion and outlook	68
A	Covariance matrix evolution	70
B	Gauge-invariant phases	72
C	Two-cavity superoperator perturbation theory	76

Abstract

We present schemes for stabilizing entangled states between bosonic cavity modes. We consider a pair of cavities connected with a nonreciprocal waveguide, realizing a cascaded quantum system. The second cavity is tuned to perfectly absorb all output of the first. Both cavities are subject to resonant two-photon parametric drives, and are equipped with optional local self-Kerr nonlinear interactions. The system is driven into a pure, unique entangled steady-state. In the case of just having parametric drives, the resulting state exhibits two-mode squeezing that can be made arbitrarily large. With Kerr nonlinearities present, we instead stabilize an entangled two-mode cat state. We show that unwanted losses in the system do not prevent us from maintaining high fidelity of $F > 0.9$ within realistic experimental parameters. We discuss the rates and time scales needed for the transient dynamics to reach this desired steady-state, and propose methods of expediting the stabilization using adiabatic ramps of the drives. Finally, we investigate the underlying theory of the perfect absorber recipe used, demonstrating the reduced role of nonreciprocity in contrast to conventional literature on the subject.

Résumé

Nous présentons des schémas pour stabiliser les états enchevêtrés entre les modes de cavité bosonique. Nous considérons une paire de cavités liées à un guide d'ondes non réciproque, réalisant un système quantique en cascade. La deuxième cavité est réglée pour absorber parfaitement tout ce qui sort de la première. Les deux cavités sont soumises à un processus paramétriques à deux photons résonnants et sont équipées d'interactions non linéaires auto-Kerr locales optionnelles. Le système mené à un état enchevêtré stable et unique. Dans le cas d'avoir simplement des processus paramétriques, l'état résultant présente une compression à deux modes qui peut être arbitrairement grande. Avec les non-linéarités de Kerr présentes, nous stabilisons plutôt un état cat à deux modes enchevêtré. Nous montrons que les pertes indésirables dans le système ne nous empêchent pas de maintenir une fidélité élevée de $F > 0,9$ avec des paramètres expérimentaux réalistes. Nous discutons des taux et échelles de temps nécessaires à la dynamique transitoire pour atteindre cet état d'équilibre souhaité, et proposons des méthodes d'accélération de la stabilisation à l'aide de rampes adiabatiques des forces paramétriques. Enfin, nous étudions la théorie sous-jacente de la recette absorbante parfaite utilisée, démontrant le rôle réduit de non-réciprocité contrairement à la littérature conventionnelle sur le sujet.

Acknowledgements

When I first applied for a master's degree, I did so to ensure that I would stay interested in research at the graduate level. Two years later, I am glad to say that the spark of passion for physics remains stronger than ever. The main reason for this is the people that I have worked with, whose support and camaraderie have transformed my understanding of science.

The first and foremost person to thank is my supervisor Aashish Clerk, who guided me from beginning to end. He always kept clear sight on the big-picture goal, while simultaneously keeping me on track with the details and ensuring that I learned in the process. His responsiveness, mentorship and range of knowledge have been an incredible source of inspiration for me.

I also want to thank Luke Govia, Rakesh Tiwari, Hugo Ribeiro, Alexander MacDonald and the others in my group for helpful discussions when I invariably got stuck or confused. They are fantastic scientists and incredible people, and it has been a pleasure to work alongside them.

Outside of the group, I am grateful to Raj Shampur, Paul Jreidini, Raphael Prentki, Alessandro Ricottone and Pericles Philipopoulos for heartfelt office discussions about both the technical and sentimental parts of graduate life. Finally, I thank my brother Alexandre Mamaev and parents Eugene Mamaev & Eugenia Mamaeva, for providing the bedrock love and support without which no part of this work could have ever come to fruition.

Contributions: All chapters were written by Mikhail Mamaev.

Chapter 1

Introduction

Can something be improved by having things taken out of it? Even in the normal world, the answer is yes. We need only look at the examples of a hole being dug in the ground, or an overly long master's thesis. But in the mysterious world of quantum mechanics, we can find answers to this question that are far more interesting.

The subject of this thesis is the generation of entangled states between cavity modes in quantum optics. There has been enormous growth in this field towards the applications of quantum information [1], quantum communications [2] and photonic networks [3]. Such states can be made more robust to imperfections and noise, because they involve the overall dynamics of an infinite-dimensional Hilbert space rather than individual degrees of freedom.

The primary experimental platform that we consider is circuit quantum electrodynamics (cQED) [4]. In contrast to more conventional cavity quantum electrodynamics, cQED replaces real interacting atoms with artificial ones. This platform has gained recent popularity for providing simple and compact ways of realizing strong coupling between circuit elements [5, 6]. It can be used to implement squeezing interactions [7, 8] and strong nonlinearities [9, 10, 11], which we will use to generate entangled states.

Entanglement is a crucial resource for any implementation of quantum computation [12], but there are still several obstacles to its generation. Any realistic quantum computer or network in quantum optics needs to have many cavities. Being able to entangle any two of

them requires some nontrivial, nonlocal interaction between each pair. This quickly grows intractable if we want to entangle cavities fast enough to do something useful with them, leading to scaling and resource issues. There has been work in the literature on creating nonlocal cavity entanglement [13, 14, 15], but the challenge of scaling has not yet been resolved.

One promising avenue for entanglement generation is the use of engineered dissipative reservoirs [16]. These allow the system to reach a steady-state exhibiting entanglement or other nonclassical properties by selectively cooling the normal modes of the system [17, 18, 19, 20, 21]. The resulting state remains stable, and can be transported for use in another part of a quantum computer when needed. However, such setups still remain resource-intensive. Even for a quadratic system with no true nonlinearities, two engineered reservoirs are needed to cool the system's normal modes, which poses a challenge for scalable experimental setups [20, 19, 21].

In this thesis, we propose two simple, low-resource systems that can create pure entangled bosonic cavity states. We only employ local interactions, avoiding the issue of scaling. Furthermore, we make use of just a single engineered dissipative reservoir, realized in the context of cascaded systems. We directionally decouple one of our cavities from the other, creating a nonreciprocal setup that maximizes the possible entanglement between the two. The first system will generate two-mode squeezed states using only quadratic, local parametric drives. The second system will extend the recipe of the first to include local Kerr nonlinearities, allowing for non-Gaussian entangled cat states to be generated. The latter has seen much recent development, as cat states provide a robust platform for universal quantum computation [22, 23, 24, 25, 26, 27, 28].

In chapter 2, we will give a short overview of the relevant background information. Chapter 3 will discuss the system that generates two-mode squeezed states. Chapter 4 will go over the entangled cat-generating system. Chapter 5 will discuss ways of expediting our system's state generation using adiabatic drive ramps.

Chapter 2

Relevant background from quantum optics

2.1 Commonly-used states

Before diving into the systems that we have designed, we give a short review of relevant material. We will first talk about the kinds of states that our cavities can be populated by. We then discuss the Lindblad master equation used to describe dissipation in the cavities. Lastly, we go over the special case of cascaded quantum systems, and show the perfect absorber recipe that can be applied to them to generate pure entangled steady-states.

2.1.1 Coherent states

The cavity in question is a resonant electromagnetic mode of an LC circuit. It is characterized by annihilation and creation operators \hat{a} , \hat{a}^\dagger , which act on the Fock-state basis $|n\rangle$, and obey the standard commutation relations of $[\hat{a}, \hat{a}^\dagger] = 1$.

The base ingredient to any more complicated state in quantum optics is the coherent state. It is defined by,

$$|\alpha\rangle = e^{-|\alpha|^2/2} \sum_{n=0}^{\infty} \frac{\alpha^n}{\sqrt{n!}} |n\rangle, \quad (2.1)$$

where α is the coherent amplitude. This state is an eigenvector of the annihilation operator, $\hat{a}|\alpha\rangle = \alpha|\alpha\rangle$. The coherent state is the closest analogue to a classical state. A driven quantum harmonic oscillator with coherent eigenstates has the equations of motion for its

expectation values mimic those of a classical harmonic oscillator.

2.1.2 Squeezed-states

A coherent state's quadratures have a fixed level of uncertainty in phase space. This uncertainty is equal for both quadratures, and satisfies the minimum amount required by the Heisenberg uncertainty principle.

However, the Heisenberg uncertainty principle is only an inequality that constrains the product of the uncertainties, not their individual values. We can thus envision a state that has less than the minimum uncertainty for one of the quadratures, at the price of having it higher than the minimum in the other quadrature [1, 29]. Such a state may be generated with the squeezing operator,

$$\begin{aligned}\hat{S}(\zeta) &= e^{\frac{1}{2}(\zeta\hat{a}\hat{a}-h.c.)}, \\ \zeta &= re^{i\theta}.\end{aligned}\tag{2.2}$$

If we act with $\hat{S}(\zeta)$ on a vacuum-state $|0\rangle$, we will get a squeezed-state. The parameter ζ controls the amplitude and phase-space axis of squeezing. In particular, for a squeezed vacuum state $\hat{S}(\zeta)|0\rangle$, we have,

$$\begin{aligned}\langle(\Delta\hat{y}_1)^2\rangle &= \frac{1}{2}e^{-2r} \\ \langle(\Delta\hat{y}_2)^2\rangle &= \frac{1}{2}e^{2r},\end{aligned}\tag{2.3}$$

where \hat{y}_1, \hat{y}_2 depend on the rotation angle θ ,

$$\begin{aligned}\hat{y}_1 &= -\cos\left(\frac{\theta}{2}\right)\hat{x} - \sin\left(\frac{\theta}{2}\right)\hat{p}, \\ \hat{y}_2 &= \sin\left(\frac{\theta}{2}\right)\hat{x} - \cos\left(\frac{\theta}{2}\right)\hat{p},\end{aligned}\tag{2.4}$$

as well as the base quadratures of the system,

$$\hat{x} = \frac{1}{\sqrt{2}}(\hat{a} + \hat{a}^\dagger), \quad \hat{p} = \frac{-i}{\sqrt{2}}(\hat{a} - \hat{a}^\dagger).\tag{2.5}$$

One way to generate a squeezed state is to use a parametric drive, implemented with a degenerate parametric down-converter [30, 31]. After all relevant approximations, the drive Hamiltonian will take the form of,

$$\hat{H}_{\text{sqz}} = \omega_c \hat{a}^\dagger \hat{a} + \lambda [e^{2i\omega_d t} \hat{a} \hat{a} + h.c.], \quad (2.6)$$

Here, ω_c is the base cavity frequency and λ is the amplitude of the parametric drive. Since this Hamiltonian is still time-dependent, we make a rotating-frame transformation,

$$\begin{aligned} \hat{H}_{\text{rsqz}} &= \hat{U}^\dagger \hat{H}_{\text{sqz}} \hat{U} - i\hat{U}^\dagger \frac{d}{dt} \hat{U}, \\ \hat{U} &= e^{-i\omega_d \hat{a}^\dagger \hat{a} t}. \end{aligned} \quad (2.7)$$

The result is,

$$\hat{H}_{\text{rsqz}} = (\omega_c - \omega_d) \hat{a}^\dagger \hat{a} + \lambda(\hat{a} \hat{a} + h.c.). \quad (2.8)$$

If we now drive on-resonance at $\omega_c = \omega_d$, we can write the time-evolution operator for the system's wavefunction,

$$\begin{aligned} |\psi(t)\rangle &= e^{-i\hat{H}_{\text{rsqz}} t} |\psi(0)\rangle \\ &= e^{\frac{1}{2}(-2i\lambda\hat{a}\hat{a}-h.c.)} |\psi(0)\rangle \\ &= \hat{S}(-2i\lambda t) |\psi(0)\rangle. \end{aligned} \quad (2.9)$$

The system's initial state becomes squeezed as a function of time.

Squeezed-states are nonclassical states of light. A single-mode squeezed state is useful for measurement protocols. If we can couple some quantity of interest to the quadrature that gets squeezed, the noise in its resulting measurement will be reduced.

Another key advantage is their ability to generate entanglement. If we have two cavities (annihilation operators \hat{a} , \hat{b}), and instead squeeze two of the four combined quadratures of the system, the resulting two-mode state will become entangled. Doing so with a direct

Hamiltonian interaction requires a nonlocal drive of the form,

$$\hat{H}_{\text{tms}} = \lambda(\hat{a}\hat{b} + h.c.) \quad (2.10)$$

The system we will describe in the next chapter will circumvent this requirement with dissipation.

Before we move on, we need to mention the issue of parametric instability. Assuming that the initial state for the above calculation was $|\psi(0)\rangle = |0\rangle$, the resulting state can be written in the Fock basis as [30],

$$\hat{S}(\zeta) |0\rangle = \mathcal{N} \sum_{n=0}^{\infty} [-e^{-i\theta} \tanh(r)]^n \sqrt{\frac{(2n-1)!!}{(2n)!!}} |2n\rangle, \quad (2.11)$$

where \mathcal{N} is a normalization constant. For \hat{H}_{rsqz} we would have $\theta = 0$, but we write the general form to make use of later.

Since the squeezing parameter of \hat{H}_{rsqz} is linearly dependent on time, then for $t \rightarrow \infty$ the coefficients of the higher Fock states will diverge. The driven system is parametrically unstable. In an experiment, this means that whatever pump or source drives the system will flood it with photons, causing the populations in the cavities to diverge. This will in turn lead to the Hamiltonian of the system breaking down, because higher-order nonlinearities will become relevant to the dynamics. This concern is exclusive to bosonic systems which have no limit to the population that each state can hold.

We can circumvent parametric instability by driving off-resonance, adding other terms to impose energy cost for excitations, or including dissipation.

2.1.3 Cat states

While the squeezed state does not have a straightforward analogue in classical mechanics, it still has a positive Wigner function. Squeezed states are Gaussian, and can be generated

with a quadratic system. We now consider a more interesting, non-Gaussian set of states.

The states we will look at are the cat states, defined by,

$$|\mathcal{C}_{\pm}(\alpha)\rangle = \frac{1}{\sqrt{2(1 \pm e^{-2|\alpha|^2})}} (|\alpha\rangle \pm |-\alpha\rangle). \quad (2.12)$$

The summed state $|\mathcal{C}_{+}(\alpha)\rangle$ is known as an even cat, whereas $|\mathcal{C}_{-}(\alpha)\rangle$ is an odd cat. The even cat has an overall even parity, only having nonzero amplitude on the Fock states $|0\rangle$, $|2\rangle$, etc. Likewise, the odd cat only inhabits $|1\rangle$, $|3\rangle$, etc.

Cat states form a superposition of two coherent states. The original Schrodinger's cat was a satirical thought experiment involving a superposition of two macroscopic states - the living and dead cat. A cat state is a more realistic implementation of this idea. Of course, instead of cat well-being, we use coherent states. Since coherent states can be related back to something classical, the cat states allow us to come closer to the idea of a macroscopic quantum superposition.

Aside from being an example of quantum phenomena in action, the cat states have seen recent uses in quantum information [22, 25]. Their superposition structure and orthogonality allows them to be used for qubits, representing a logical zero state with the even cat and a logical one with the odd cat (or vice-versa).

Cat states are harder to generate than squeezed or coherent states. Since they are non-Gaussian, they require true nonlinear interactions. Implementations exist using homodyne detection on number states [32], laser pulse down-conversion [33], quantum nondemolition measurements [34] and others discussed in Ref. [30].

Older work has made use of Kerr nonlinear interactions to make cats at specific time snapshots during transient evolution [35]. This thesis will use Kerr nonlinearities to stabilize entangled cat states in the steady-state, which will be discussed in Chapter 4.

2.1.4 Wigner function

All the cavity states described in the previous sections have an inherent uncertainty in their quadratures due to the Heisenberg uncertainty principle. We can quantify this uncertainty with the Wigner function [36], which is a quasiprobability distribution describing a state in its two-dimensional phase space.

The two components of the phase space are the quadrature eigenvalues x, p for the continuous-variable operators $\hat{x} = (\hat{a} + \hat{a}^\dagger)/\sqrt{2}$, $\hat{p} = -i(\hat{a} - \hat{a}^\dagger)/\sqrt{2}$. For a density matrix ρ in the Fock basis, the Wigner function of $\alpha = x + ip$ is defined by,

$$\begin{aligned} W(\alpha) &= 2\text{tr} \left[\rho D(\alpha) e^{i\pi \hat{a}^\dagger \hat{a}} D^\dagger(\alpha) \right], \\ D(\alpha) &= e^{\alpha \hat{a}^\dagger - \alpha^* \hat{a}} \end{aligned} \tag{2.13}$$

Here, $D(\alpha)$ is the displacement operator. For a classical harmonic oscillator, the displacement operator simply takes the system from the origin to the point α . In the quantum case, we will instead generate a coherent state of amplitude α .

The reason that we refer to the Wigner function as a quasiprobability distribution is because certain states can cause it to take on negative values. Having a negative Wigner function indicates that the state exhibits strongly non-classical properties such as superposition, and is an indicator of non-Gaussian states. The negativity of the Wigner function can be used as a metric of how ‘quantum’ a particular state is.

Fig. 2.1 shows sample Wigner function plots for the three types of states discussed in this subsection. Note that the cat state has interference fringes resulting from the superposition structure.

We also note that there are other quasiprobability distributions used to describe cavity mode states, such as the P-representation [36] or the Q-function [37].

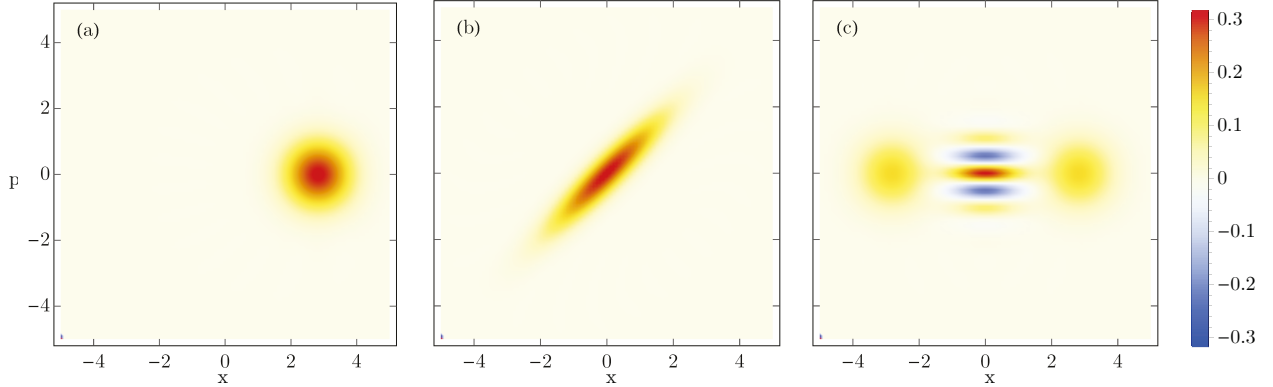


Figure 2.1: (a) Wigner function of a coherent state $|\alpha\rangle$ with $\alpha = 2$. (b) Wigner function of a squeezed vacuum state $S(\zeta)|0\rangle$, with squeeze parameter $\zeta = 0.8e^{i\pi/2}$. (c) Wigner function of an even cat state $|\mathcal{C}_+(\alpha)\rangle$ with amplitude $\alpha = 2$.

2.2 Lindblad master equation

2.2.1 Equation form

In any realistic experiment, there will be external noise and dissipation. We can minimize these through the use of vacuum chambers or very low temperatures, but it is not possible to completely isolate the fragile quantum degrees of freedom. Any cQED setup will have some leakage rate due to imperfect isolation of the circuit elements. Including nontrivial Hamiltonian terms provides additional complexity to the system, which brings more potential sources of dissipation. Above all, photons need to be able to leave the system if we want to measure it.

Unwanted dissipation involves the coupling of our cavity to a thermal bath or reservoir. This reservoir typically involves an enormous number of excitations and degrees of freedom. Solving for analytic dynamics with its full Hilbert space becomes intractable.

What we do instead is describe the system's evolution without fully understanding what happens to the bath. We trace out the bath degrees of freedom, leaving just a modified equation for the density matrix that incorporates the effect of the bath into the dynamics. Since we do not keep in the information about the bath itself, its action on the system becomes stochastic in nature. Instead of deterministic coherent evolution, our system will undergo a

probabilistic one, described by a master equation. Under a series of approximations, which will be discussed in the next subsection, we can simplify the result down into a well-known form known as the Lindblad master equation [38].

Note that this thesis will not go into the full mathematical details. A quantum jump-based derivation is given in Ref. [39], while microscopic derivations are discussed in Refs. [40, 41, 42].

The Lindblad master equation for a quantum system with Hamiltonian \hat{H} takes the form of,

$$\begin{aligned} \frac{d}{dt}\rho &= -i[\hat{H}, \rho] + \sum_k \gamma_k \mathcal{L}[\hat{z}_k]\rho, \\ \mathcal{L}[\hat{z}]\rho &= \hat{z}\rho\hat{z}^\dagger - \frac{1}{2}\hat{z}^\dagger\hat{z}\rho - \frac{1}{2}\rho\hat{z}^\dagger\hat{z}. \end{aligned} \tag{2.14}$$

The first term is just the ordinary, coherent evolution due to the system Hamiltonian. The second terms represent different dissipative processes, which can also be called ‘decay channels’. The coefficients γ_k tell us the rate at which each decay process occurs. The operators \hat{z}_k are called jump operators. Their original role was to describe how the system couples to the environment. They now represent the way that the reservoir acts on the system to induce dissipation. The simplest example of a jump operator is just a cavity annihilation operator, $\hat{z} = \hat{a}$. Such a decay channel would involve photons hopping from the cavity into the modes of the reservoir, one at a time. More complicated examples can involve subtracting more than one photon at a time, or having correlated dissipation involving more than one cavity.

The Lindblad superoperator $\mathcal{L}[\hat{z}]$ acts on the density matrix. Its first term represents the action of the bath on the system. The second two terms in the Lindblad superoperator can be thought of as measurements. When the bath acts with its jump operator, it simultaneously makes a measurement of the system state.

The Lindblad equation is the *only* form of a master equation that is guaranteed to be completely positive and trace preserving at all times, for any initial conditions. This key property allows the system density matrix to remain a density matrix regardless of the initial condition.

One more thing to note is that we will often be interested in the *steady-state* solution, which is the density matrix that satisfies:

$$\frac{d}{dt}\rho_{\text{st}} = 0. \quad (2.15)$$

The bath will tend to push or relax the system into a state where any driving or coherent terms in the Hamiltonian are perfectly balanced against the dissipation. The steady-state represents what the system will look like in the infinite-time limit. This is useful information, because a steady state is far easier to understand and measure than a transient one. Instead of having to predict the evolution and measure it at just the right time, all we have to do to reach the steady-state is set the system up and wait.

Bear in mind that steady-states are not always unique. If there is some symmetry in the system, such as parity symmetry, different initial conditions for the evolution will lead to different final results. These symmetries can be mapped back to conserved quantities in the system. See Ref. [43] for details.

We also note that steady-states are not guaranteed to exist. As a rule of thumb, if there are coherent oscillations in the system due to its internal Hamiltonian \hat{H}_S , all the oscillating degrees of freedom must have some way of connecting back to the dissipation to be relaxed into a steady-state. This connection can be a direct jump operator that couples to a bath, or indirect, such as a coherent coupling to another degree of freedom that is damped. There can be more esoteric systems that have no steady-state despite satisfying the above requirements. For the cavity systems we will be considering, the rule of thumb is good enough.

2.2.2 Superoperator formalism

The general master equation in Eq. (2.14) tends to be very difficult to solve. The superoperator acts on the density matrix in a nontrivial way. To make things a little more transparent, it is helpful to collect both the coherent Hamiltonian terms and dissipators into a single large

superoperator,

$$\frac{d}{dt}\rho = L\rho, \quad (2.16)$$

where $L\rho$ equals the right hand side of equation (2.14). L is called the Liouvillian superoperator. As suggested by the above equation, the master equation is really just a simple first-order linear system, albeit of a larger size than the density matrix itself. We can see this by re-writing the density matrix as a vector,

$$\begin{aligned} \rho &= \begin{pmatrix} c_1 & \dots & c_N \end{pmatrix}, \\ \rho_v &= \begin{pmatrix} c_1 \\ \vdots \\ c_N \end{pmatrix}, \end{aligned} \quad (2.17)$$

where c_j are the $N \times 1$ columns of ρ , assuming it is of dimension N . The subscript v will be used from this point onwards to indicate this column-stacking operation. In this context, the master equation can be rewritten as,

$$\frac{d}{dt}\rho_v = L\rho_v, \quad (2.18)$$

where the Liouvillian superoperator becomes,

$$L = -i(\mathbb{1}_N \otimes \hat{H} - \hat{H}^* \otimes \mathbb{1}_N) + \sum_k \gamma_k \left(\hat{z}^* \otimes \hat{z} - \frac{1}{2}\mathbb{1}_N \otimes \hat{z}^\dagger \hat{z} - \frac{1}{2}(\hat{z}^\dagger \hat{z})^* \otimes \mathbb{1}_N \right). \quad (2.19)$$

From this structure it is evident that our column-stacking has allowed us to decompose the actions of the Liouvillian on the left and right portions of the density matrix outer product.

The purpose of this transformation is to make the master equation easier to solve. While the size of the involved matrices is now N^2 rather than N , it is a simple linear algebra problem. Finding the steady-state(s) corresponds to finding the null space of L . Information about the transient dynamics can be obtained from the nonzero eigenvalues of L . Despite

the large dimension of the matrix, it is very sparse due to the tensor product structure. This allows for the usage of powerful numeric techniques such as Arnoldi iteration [44] which have been developed over the years for linear systems.

2.3 Cascaded systems

2.3.1 Overview

Classical circuits contain elements such as circulators and isolators, which feature nonreciprocal dynamics. They cause some part of the system to act upon another part, without being responded to in kind. We want to replicate these nonreciprocal dynamics in cQED because they can be used for entanglement generation [45, 46, 47], as well as a wide berth of other applications [48, 49, 50, 51, 52, 53, 54]

To have nonreciprocal physics in a quantum system, we require dissipation. Hamiltonian dynamics are insufficient, because any coherent coupling or tunneling term must have a Hermitian conjugate counterpart allowing the opposite process. There are cases where non-Hermitian Hamiltonians can be considered [55], but these can often be mapped back to a dissipative process. For example, the photon number-measuring part of the Lindblad superoperator [the last two terms on the right hand side of Eq. (2.14)] can be thought of as a non-Hermitian Hamiltonian $-i\hat{z}^\dagger\hat{z}/2$.

In this section we will describe cascaded quantum systems [56, 57], which are an example of maximal nonreciprocity. Fig. 2.2(a) shows a qualitative depiction of how a cascaded system can look. There are two subsystems, labelled A and B. Information and/or excitations can leak out of one part into the other, but not vice versa. It can be thought of as a one-way mirror, where system B can see A and be influenced by its state. System A, on the other hand, sees only itself and obeys equations of motion that do not involve B in any way. Cascaded quantum systems are not constrained to two parts, and one can envisage an entire chain of them, with information cascading down the line in one direction.

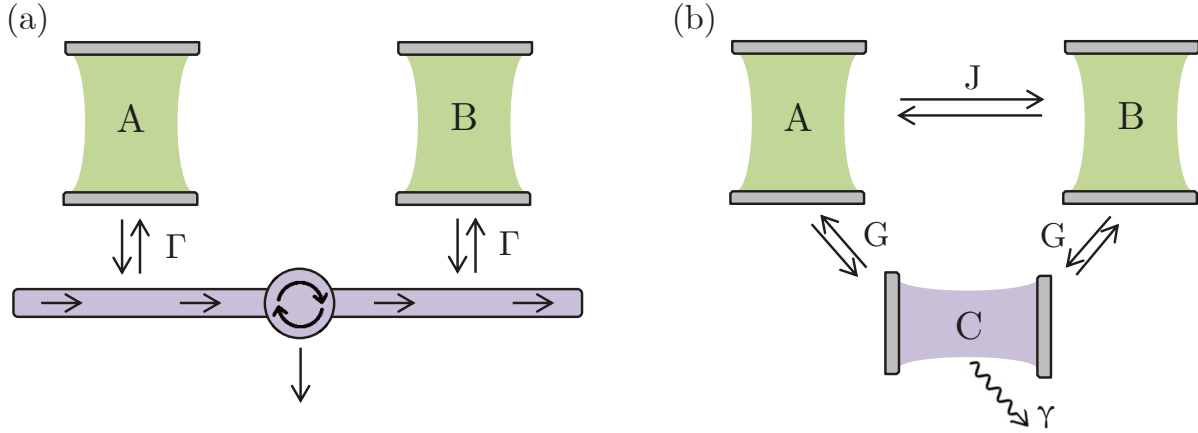


Figure 2.2: (a) Schematic diagram of a nonreciprocal system implemented with a circulator. Two parts, labelled A and B, are connected with a chiral waveguide. Signals can only propagate down the waveguide in one direction. Both parts couple to the waveguide with some equal rate Γ , and corresponding jump operator \hat{z}_A (\hat{z}_B) for system A (B). (b) Schematic of a synthetic nonreciprocal system. There is a direct coherent coupling with strength J between the main cavities. An auxiliary cavity C acts as an effective nonlocal reservoir. The auxiliary cavity is heavily damped with some rate γ , and tunnel-coupled to the cavities A, B with rate G . The couplings to C are pump-mediated to allow a relative phase of $\pi/2$ between the two coherent terms. This system corresponds to (a) in the limit of $G/J \gg 1$ and $\gamma/J \gg 1$ in such a way that $J = \Gamma = 4G^2/\gamma$ [58].

2.3.2 Master equation

A two-part cascaded system can be described by a simple Lindblad master equation. We assume that there are two cavities (annihilation operators \hat{a}, \hat{b}) connected by a chiral waveguide. This waveguide acts as a reservoir with some correlation between its actions on the cavities, resulting in the cancelling out of all signals from A to B. While there is no truly chiral waveguide in quantum optics, we can obtain an effective one through the use of circulators that remove any back-scattering processes. See Refs. [59, 60] for sample implementations of a circulator, and Refs. [61, 62] for theoretical discussions.

As in the previous sections, we will omit detailed derivations. The relevant equations of motion can be obtained using the SLH formalism (not an acronym) [61] or input-output theory [63]. After tracing out the waveguide, we are left with an effective master equation

of the form,

$$\begin{aligned}\hat{H}_{\text{nr}} &= \hat{H}_A + \hat{H}_B + J(\hat{z}_A^\dagger \hat{z}_B + h.c.), \\ \frac{d}{dt}\rho &= -i[\hat{H}_{\text{nr}}, \rho] + 2J\mathcal{L}[\hat{z}_A \pm i\hat{z}_B]\rho.\end{aligned}\tag{2.20}$$

The two Hamiltonians \hat{H}_A , \hat{H}_B contain the internal dynamics of cavity A and B respectively. The jump operators \hat{z}_A , \hat{z}_B describe the coupling of the waveguide to the cavity with amplitude J . The simplest case, as seen before, is just single-photon tunneling $\hat{z}_A = \hat{a}$. The sign of the phase inside the dissipator tells us which way the directionality goes. A minus sign is left to right, and plus is right to left.

We see that mandating the waveguide to be chiral induces both a coherent Hamiltonian coupling, and a nonlocal dissipator. The coherent coupling is a virtual waveguide-mediated term that describes photons leaking from A into B through the waveguide. Normally, the reverse process would also be possible. However, the nonlocal dissipator can be expanded out to contain correlation terms which exactly cancel out the B to A tunneling terms. This is the reason for them both having the same prefactor J - they come from the same waveguide. Note that the factor of two for the dissipator comes from the $1/2$ in the Lindblad superoperator's definition.

The nonreciprocity leads to a directional decoupling of cavity A. It can be described by a reduced master equation involving only itself,

$$\frac{d}{dt}\rho_A = -i[\hat{H}_A, \rho_A] + J\mathcal{L}[\hat{z}_A]\rho_A,\tag{2.21}$$

where ρ_A is the reduced density matrix for cavity A. Cavity A thus knows nothing about B, and cannot be affected by its state. We can obtain analytic information about the system more easily, because we only have one cavity to worry about. However, the key thing to note is that we can still have *entanglement* between the two cavities despite this directional decoupling. We will take advantage of this property in the next chapter, when we define our system of interest.

A qualitative demonstration of this directional decoupling is given in Fig. 2.3. The time evolution of the Wigner function is plotted for cavities coupled to a waveguide with single-photon tunneling. The first cavity along the waveguide is subject to parametric driving $\hat{H}_A \sim (\hat{a}\hat{a} + h.c.)$, while the second cavity has a more complex nonlinear self-Kerr interaction [64] of the form $\hat{H}_B \sim \hat{b}^\dagger \hat{b}^\dagger \hat{b} \hat{b}$. We see that regardless of the initial conditions for B, cavity A obeys simple dynamics that drive it towards a squeezed state (as we would expect from Subsec. 2.1.2). Cavity B displays more complex nonlinear dynamics that do not affect cavity A despite a coherent coupling between the two systems, due to the nonreciprocity.

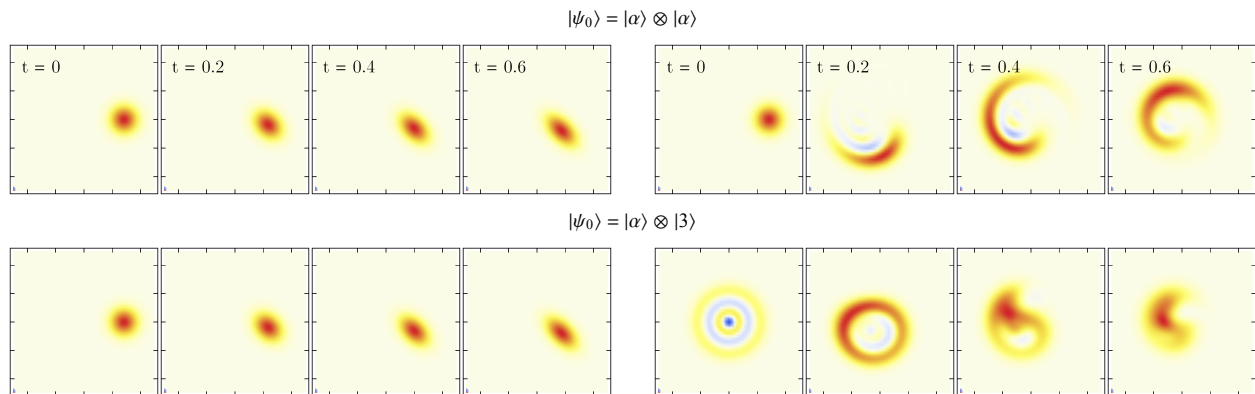


Figure 2.3: Wigner function evolution for a directionally decoupled system for different initial conditions. The system obeys the master equation in Eq. (2.20), with $\hat{H}_A = 0.4(\hat{a}\hat{a} + h.c.)$ and $\hat{H}_B = \hat{b}^\dagger \hat{b}^\dagger \hat{b} \hat{b}$ (in units of $J = 1$). The waveguide couples to the cavities with single-photon tunneling, $\hat{z}_A = \hat{a}$, $\hat{z}_B = \hat{b}$. The left panels depict the Wigner function of the cavity A density matrix $\rho_A = \text{tr}_B \rho$, while the right panels show $\rho_B = \text{tr}_A \rho$. The top set of panels corresponds to an initial condition $|\psi_0\rangle$ of both cavities starting in coherent states $|\alpha\rangle$ with amplitude $\alpha = 2$. The bottom panels start with cavity A in the same coherent state $|\alpha\rangle$, while cavity B is initialized in a Fock state $|3\rangle$ instead.

2.3.3 Synthetic implementations

One last thing to point out is that cascaded systems do not need a true chiral waveguide. The nonreciprocity requires a coherent coupling and nonlocal dissipator, matching their prefactor coefficients to obtain the necessary cancellation. If we do have a chiral waveguide, it will ‘provide’ both terms simultaneously. However, more recent work on non-reciprocal systems has observed that these two pieces can be attached separately to achieve the same effect [58].

We consider a coherent coupling between our two cavities,

$$\hat{H}_J = J(\hat{z}_A^\dagger \hat{z}_B + h.c.), \quad (2.22)$$

as well as a dissipation term,

$$\mathcal{L}_\Gamma = 2\Gamma\mathcal{L}[\hat{z}_A \pm i\hat{z}_B]. \quad (2.23)$$

If we then tune these two independent terms to match,

$$\Gamma = J, \quad (2.24)$$

we will get a nonreciprocal system. Note that we have included the factor of two in the dissipator definition, so that the coherent coupling and dissipation can be compared directly.

The coherent coupling is no longer a virtual waveguide-mediated term, but now a real Hamiltonian term. The advantage of this method is that we have more control over experimental implementation. Making a chiral waveguide is difficult because it requires circulators, which are bulky and prone to high levels of loss. On the other hand, coupling two cavities can be done in a variety of ways without significant levels of imperfection. Creating the non-local dissipator is also straightforward. Several implementations are discussed in Ref. [58]. As seen in Fig. 2.2(b), the dissipator can be as simple as a damped auxiliary third cavity coupled to the other two [58, 65]. We have to pump-mediate the couplings to the other cavities to get the relative phase of $\pm\pi/2$. Such an implementation would not be subject to circulator transmission losses, suffering only from leakage from the cavities instead (which is orders-of-magnitude smaller). We will see this implementation explicitly in Sec. 3.3.

2.4 Perfect absorber recipe

Cascaded quantum systems can be used to generate entanglement. Excitations in subsystem A can be correlated to one another. When these leak down the waveguide and enter B, the

correlations persist. Nonreciprocity assures that the reverse process is impossible. However, excitations can leak further down the waveguide into the environment, destroying the cavity-cavity entanglement. We want everything emitted by A to be caught by B, and for nothing to leak out of B.

The way to do so is a recent technique for cascaded systems known as the perfect-absorber recipe [66]. The idea behind it is to tune the Hamiltonian of cavity B so that it absorbs all of the signals emitted by A in the steady-state. As a result, nothing escapes further into the waveguide, and the only entanglement can be between the two cavities.

Moreover, the resulting steady-state will become *pure*, because the environment effectively plays no role in the infinite-time limit. This makes it both easier to deal with mathematically, and more desirable, because we want to generate pure entangled states for quantum computing.

The steady-state for such a setup is a dark-state of the dissipator, as defined by,

$$(\hat{z}_A - i\hat{z}_B) |\psi\rangle = 0. \quad (2.25)$$

Note that we assumed a left-to-right chirality, and will continue to do so unless otherwise stated. If we want this to be the steady-state for our system, we also need it to be an eigenstate of the overall Hamiltonian,

$$\hat{H}_{\text{nr}} |\psi\rangle = E |\psi\rangle, \quad (2.26)$$

where E is some constant eigenvalue.

The explicit perfect absorber recipe for solving system A's isolated master equation then proceeds as follows:

1. We start with a known Hamiltonian \hat{H}_A , coupled to a chiral waveguide with a jump operator \hat{z}_A .

2. We connect another system further along the waveguide with jump operator \hat{z}_B (assuming nothing about its Hamiltonian for the time being).
3. We find an *ansatz* for a pure state $|\psi\rangle$ that satisfies Eq. (2.25).
4. We find a Hamiltonian \hat{H}_B such that the state $|\psi\rangle$ satisfies Eq. (2.26).

The end result will be a system that must necessarily be driven into the pure steady-state $|\psi\rangle$. As we will see in the following chapters, this state can be made entangled.

The last step in the above recipe may sound daunting at first. There is a general approach described in Ref. [66]. However, as described in the same reference, an easier way is to assume a system-B Hamiltonian that mirrors system-A, up to a change in term amplitudes. For instance, if system A had a Hamiltonian term of $\hat{H}_A \simeq \lambda_A(\hat{a}\hat{a} + h.c.)$, we would assume that system B obeys the same form, $\hat{H}_B \simeq \lambda_B(\hat{b}\hat{b} + h.c.)$. An explicit example of how this works will be shown in the following subsection. What we then do is act on our dark-state ansatz $|\psi\rangle$ with our assumed Hamiltonian. If we are able to find coefficients for the ansatz and Hamiltonian parameters that make the result an eigenstate, then the problem is solved.

Note that in principle, we do not care about the energy of the overall resulting eigenstate. In practice, the easiest state to search for is a zero-energy eigenstate, $E = 0$.

As an additional note, the perfect absorber recipe is also an easy way of solving for the steady-state of a Lindblad master equation. Recall that the directional decoupling means that cavity A obeys its own reduced equation of motion [c.f. Eq. (2.21)]. If we wanted to know just the solution to that master equation alone, we could apply the perfect absorber recipe to find the pure steady-state of the two-cavity system. The impure steady-state for just A can then be obtained by tracing over B.

Chapter 3

Two-mode squeezing via broken time-reversal symmetry

Now that the stage is set, we move on to describing our first entanglement-generating system of interest. We are going to apply the perfect absorber recipe to cavities with parametric driving. The goal is to make a Gaussian pure entangled state. While this requires two reservoirs in conventional literature [20, 19, 21], we will only use one.

We assume that our cavities couple to a chiral waveguide with simple single-photon tunneling, resulting in a Hamiltonian and master equation of,

$$\begin{aligned}\hat{H}_{\text{PD}} &= \hat{H}_{\text{A}} + \hat{H}_{\text{B}} + J(\hat{a}^\dagger \hat{b} + h.c.), \\ \frac{d}{dt}\rho &= -i[\hat{H}_{\text{PD}}, \rho] + 2J\mathcal{L}[\hat{a} - i\hat{b}]\rho.\end{aligned}\tag{3.1}$$

Both cavities are parametrically driven on-resonance, resulting in rotating-frame Hamiltonians given by,

$$\begin{aligned}\hat{H}_{\text{A}} &= \lambda_{\text{A}}(\hat{a}\hat{a} + h.c.), \\ \hat{H}_{\text{B}} &= \lambda_{\text{B}}(e^{i\phi}\hat{b}\hat{b} + h.c.).\end{aligned}\tag{3.2}$$

Here, λ_{A} and λ_{B} are the parametric drive amplitudes. Fig. 3.1 gives a qualitative depiction of the setup. The reason that we drive both cavities is because the perfect absorber recipe requires a degree of symmetry between the two systems [66]. The terms present on cavity A

must be mirrored by cavity B, up to choices of coefficients.

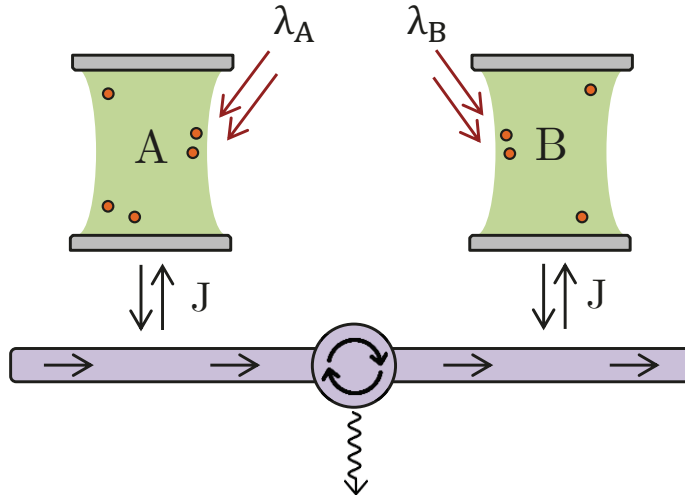


Figure 3.1: Parametrically driven two-cavity setup from Eq. (3.1), assuming an explicit chiral waveguide implementation. Both drives add photons in pairs. The waveguide only allows information to propagate in one direction, creating both a dissipator and waveguide-mediated coherent coupling.

Note that we have also assumed an arbitrary phase ϕ in the second cavity Hamiltonian, because the amplitude of the parametric drive can be complex in general. We cannot choose a gauge where both drives are always guaranteed to be real, because a gauge transformation $\hat{b} \rightarrow e^{-i\phi/2}\hat{b}$ could change the coherent coupling term and dissipator phase of Eq. (3.1), breaking the nonreciprocity. See Appendix B for details on the gauge-invariant phases in the system.

Based on our prior intuition, it is already easy to see why this system can exhibit entanglement. The parametric drive adds photons to cavity A in pairs. If one of the two tunnels over to cavity B through the waveguide, phase information will be retained between them because they were added by the same interaction. Due to the nonreciprocity, this mandates that the two photons now become entangled. The harder we drive, the more of these pairs will be added to the system.

The resulting states will have entanglement in the form of two-mode squeezing. Photons are added to A in pairs and one of the two can tunnel to B, realizing an effective nonlocal parametric. Since we are considering a quadratic system with only squeezing terms, there is

not much else that could be generated, aside from coherent displacements or phase-space rotations. Two-mode squeezed states are useful for applications in quantum teleportation [67, 68, 69], dense coding [70] and phase measurements [71]. The entanglement that they exhibit is also a general resource with wide applications to other quantum systems.

We mentioned earlier that a two-mode squeezed state would need a nonlocal drive of the form in Eq. (2.10) [72]. A cascaded system in conjunction with the perfect-absorber recipe will allow us to circumvent this requirement.

3.1 Perfect absorber recipe

We will now work out the perfect-absorber recipe of Sec. 2.4 explicitly. We look for an ansatz of a two-mode state that is a dark state of the $(\hat{a} - i\hat{b})$ dissipator jump operator. This is a lot easier if we make a basis change to normal modes,

$$\hat{c}_{\pm} = \frac{1}{\sqrt{2}}(\hat{a} \mp i\hat{b}). \quad (3.3)$$

A dark-state of our dissipator will just be any vacuum state of the \hat{c}_+ mode, with any arbitrary state in the \hat{c}_- mode. The ansatz we use is then,

$$|\psi\rangle = |0\rangle_+ \otimes \sum_{n=0}^{\infty} \alpha_n |n\rangle_-, \quad (3.4)$$

where $|n\rangle_{\pm}$ are the Fock states for the \hat{c}_{\pm} mode, and α_n are arbitrary normalized state coefficients.

We can also write our Hamiltonian in this new basis,

$$\hat{H}_{\text{PD}} = -iJ(\hat{c}_+^{\dagger}\hat{c}_- - h.c.) + \frac{1}{2} [(\lambda_A - e^{i\phi}\lambda_B)(\hat{c}_+\hat{c}_+ + \hat{c}_-\hat{c}_-) + h.c.] + [(\lambda_A + e^{i\phi}\lambda_B)\hat{c}_+\hat{c}_- + h.c.]. \quad (3.5)$$

In this basis, our Hamiltonian has both single-mode and two-mode squeezing terms. All that

remains now is step 4, to find coefficients that make $|\psi\rangle$ an eigenstate of \hat{H}_{PD} . We act with \hat{H}_{PD} onto $|\psi\rangle$ to find:

$$\begin{aligned} \hat{H}_{\text{PD}} |\psi\rangle &= |0\rangle_+ \otimes \sum_{n=0}^{\infty} \frac{\alpha_n}{2} \left[(\lambda_A - e^{i\phi} \lambda_B) \sqrt{n(n-1)} |n-2\rangle_- + (\lambda_A - e^{-i\phi} \lambda_B) \sqrt{(n+1)(n+2)} |n+2\rangle_- \right] \\ &+ |1\rangle_+ \otimes \sum_{n=0}^{\infty} \alpha_n \left[-iJ\sqrt{n} |n-1\rangle_- + (\lambda_A + e^{-i\phi} \lambda_B) \sqrt{n+1} |n+1\rangle_- \right] \\ &+ |2\rangle_+ \otimes \sum_{n=0}^{\infty} \sqrt{2} \alpha_n (\lambda_A - e^{-i\phi} \lambda_B) |n\rangle_- . \end{aligned} \tag{3.6}$$

The goal is to turn the right hand side of the above equation into a scalar multiple of $|\psi\rangle$. Instead of diving into explicit math, we can figure out the answer just by inspection. The result has been suggestively split into three pieces, corresponding to the different Fock states of c_+ . The $|0\rangle_+$ -proportional states come from the effective local parametric driving on the \hat{c}_+ mode, whereas the $|2\rangle_+$ terms are the \hat{c}_- drive. The $|1\rangle_+$ terms are all the nonlocal processes in the \hat{c}_{\pm} basis.

Since $|\psi\rangle$ is only proportional to $|0\rangle_+$, then the $|1\rangle_+$ and $|2\rangle_+$ terms must vanish to have an eigenstate.

The $|2\rangle_+$ term can only vanish if its constant prefactor vanishes. We cannot say that $\alpha_n = 0$, because we are looking for non-trivial eigenstates. This immediately imposes a condition on our system parameters,

$$\lambda_A - e^{-i\phi} \lambda_B = 0. \tag{3.7}$$

Since the coefficients λ_A and λ_B were defined to be real, the only possible choice is a phase of $\phi = 0$ and drive strengths that are equal in magnitude,

$$\begin{aligned} \phi &= 0, \\ \lambda_A &= \lambda_B = \lambda. \end{aligned} \tag{3.8}$$

Note that choosing $\phi = \pi$ instead would also work, but it would just mean that $\lambda_A = -\lambda_B$ and yield exactly the same Hamiltonian.

Upon making this variable restriction, the $|0\rangle_+$ term also vanishes. This comes from the fact that the effective local parametric driving terms we get have the same amplitude. Furthermore, since the $|2\rangle_+$ term only had one component, there was no other way to get rid of it. Thus the solution we pursue is unique, and can only correspond to a zero-energy eigenstate.

All we are left with is the $|1\rangle_+$ -proportional term,

$$\begin{aligned} \hat{H}_{\text{PD}} |\psi\rangle &= |1\rangle_+ \otimes \sum_{n=0}^{\infty} \alpha_n \left(-iJ\sqrt{n} |n-1\rangle_- + 2\lambda\sqrt{n+1} |n+1\rangle_- \right) \\ &= |1\rangle_+ \otimes \sum_{n=0}^{\infty} \left(-iJ\sqrt{n+1}\alpha_{n+1} + 2\lambda\sqrt{n}\alpha_{n-1} \right) |n\rangle_-, \end{aligned} \quad (3.9)$$

which must vanish. This can be solved by choosing the right nontrivial coefficients α_n , which must satisfy a recursion relation,

$$\alpha_{n+1} = \frac{-2i\lambda}{J} \sqrt{\frac{n}{n+1}} \alpha_{n-1}. \quad (3.10)$$

Note that this is a second-order recursion relation, which means that there are two possible solutions. The even-numbered coefficient solution is given by,

$$\alpha_{2n} = \left(\frac{-2i\lambda}{J} \right)^n \sqrt{\frac{(2n-1)!!}{(2n)!!}} \alpha_0. \quad (3.11)$$

At first, we can go through and find the solution to the odd-numbered coefficients as well. However, it pays to be very careful here. Consider the $n = 1$ term for the sum in Eq. (3.9), which contains $-iJ|0\rangle_-$. This term cannot be cancelled out, because the term that would normally be responsible for doing so corresponds to $n = -1$, and our sum starts from zero. The even-numbered coefficients do not run into this problem, but the odd ones do. There is

thus only *one* unique solution to the recursion relation.

As an aside, we note that the simultaneous cancellation of the $|0\rangle_+$ and $|2\rangle_+$ terms is only possible because both of our cavities are coupled to the waveguide with the same amplitude J . If this were not the case, we would not be able to find any perfect absorber dark-state solution.

At this point, we have found a unique state that is both a dark-state of the dissipator and a zero-energy eigenstate of the Hamiltonian, meaning that it is the steady-state of the system. Absorbing the coefficient α_0 into a normalization constant, we can then write the state,

$$|\psi_{\text{PD}}\rangle = \mathcal{N} |0\rangle_+ \otimes \sum_{n=0}^{\infty} \left(\frac{-2i\lambda}{J} \right)^n \sqrt{\frac{(2n-1)!!}{(2n)!!}} |2n\rangle_-,$$

$$\mathcal{N} = \left(1 - \frac{4\lambda^2}{J^2} \right)^{\frac{1}{4}}.$$
(3.12)

The constant \mathcal{N} normalizes the state.

While this state may not look very intuitive at first, we can re-express it in a much more familiar form using Eq. (2.11),

$$|\psi_{\text{PD}}\rangle = |0\rangle_+ \otimes e^{\frac{1}{2}(\zeta\hat{c}_- - \hat{c}_- - h.c.)} |0\rangle_- = |0\rangle_+ \otimes \hat{S}(\zeta) |0\rangle_-,$$

$$\zeta = -i \operatorname{arctanh} \left(\frac{2\lambda}{J} \right).$$
(3.13)

The steady-state is simply a squeezed vacuum state of the c_- mode, with c_+ remaining in vacuum. While this looks like a single-mode squeezed state, recall that we are working in a nonlocal basis. When we convert back to the cavity A, B basis in the next section, we will see two-mode squeezing correlations. This is analogous to a beam-splitter operation: Squeezed light sent into one arm of a beam-splitter will come out with entangled two-mode squeezing.

Something far more surprising is that looking back at the Hamiltonian in Eq. (3.5), we see that our choice of parameters ends up cancelling out the single-mode \hat{c}_- parametric driving

terms. Yet in the steady-state, we get a single-mode squeezed state of the c_- mode. This is a result of the interplay between the driving and dissipation. We have a nonlocal parametric drive that adds excitations to both modes simultaneously, but the dissipation takes away the ones in the c_+ mode, keeping it in the vacuum as the system equilibrates.

Before we move on to characterize the state, we will write out the full system with all the parameter restrictions,

$$\begin{aligned}\hat{H}_{\text{PD}} &= \lambda(\hat{a}\hat{a} + \hat{b}\hat{b} + h.c.) + J(\hat{a}^\dagger\hat{b} + h.c.), \\ \frac{d}{dt}\rho &= -i[\hat{H}_{\text{PD}}, \rho] + 2\Gamma\mathcal{L}[\hat{a} - i\hat{b}]\rho.\end{aligned}\tag{3.14}$$

This is the system whose steady-state we will characterize in the next section.

3.2 Squeezed-state properties

3.2.1 Cavity mode basis and two-mode squeezing

Now that we have the unique, exact steady-state for the parametrically driven system, we can start to examine its properties. We first rewrite it in the cavity mode basis to find,

$$\begin{aligned}|\psi_{\text{PD}}\rangle &= e^{\frac{1}{2}(\zeta\hat{a}\hat{a}-h.c.)}e^{\frac{1}{2}(-\zeta\hat{b}\hat{b}-h.c.)}e^{(i\zeta\hat{a}\hat{b}-h.c.)}|0\rangle_{\text{A}} \otimes |0\rangle_{\text{B}} \\ &= \hat{S}_{\text{A}}(\zeta)\hat{S}_{\text{B}}(-\zeta)\hat{S}_{ab}(i\zeta)|0\rangle_{\text{A}} \otimes |0\rangle_{\text{B}}.\end{aligned}\tag{3.15}$$

Here \hat{S}_{A} and \hat{S}_{B} are single-mode squeezing operators for cavity modes \hat{a} , \hat{b} respectively [c.f. Eq. (2.2)]. The operator \hat{S}_{ab} is the two-mode squeezing operator, defined by [1],

$$\hat{S}_{ab}(\zeta) = e^{\zeta\hat{a}\hat{b}-h.c.}.\tag{3.16}$$

We will quantify the entanglement of this state in Subsec. 3.2.4, but qualitatively, the state gets more entangled as $|\zeta|$ increases.

We see that both single-mode and two-mode squeezing correlations are generated. What makes this result useful is that the two-mode squeezing was made by only applying local drives. This avoids the difficulty of creating a two-mode squeezing Hamiltonian between two cavities that could be physically separated by significant distance in an experiment.

In what follows, we will derive further analytic results about the state $|\psi_{\text{PD}}\rangle$.

3.2.2 Covariance matrix

The properties of state in Eq. (3.15) can be obtained from the system's steady-state covariance matrix. Since the system was described by a quadratic master equation, the state $|\psi\rangle$ is Gaussian. This means that it is completely characterized by all of its one and two-point correlators. For two modes, these quantities can be described with a single 4×4 matrix,

$$\begin{aligned} C_{jk} &= \langle \psi_{\text{PD}} | \hat{c}_j \hat{c}_k | \psi_{\text{PD}} \rangle, \\ \hat{c}_k &= \{\hat{x}_A, \hat{p}_A, \hat{x}_B, \hat{p}_B\}. \end{aligned} \tag{3.17}$$

The operators \hat{x}_K, \hat{p}_K are the quadratures of the individual cavity modes,

$$\begin{aligned} \hat{x}_K &= \frac{1}{\sqrt{2}} (\hat{K} + \hat{K}^\dagger), \\ \hat{p}_K &= \frac{-i}{\sqrt{2}} (\hat{K} - \hat{K}^\dagger). \end{aligned} \tag{3.18}$$

For quadratic systems, the covariance matrix can be found without having to solve the master equation (c.f. Appendix A). For our setup, we find,

$$C = \frac{1}{2(J^2 - 4\lambda^2)} \begin{pmatrix} J^2 & -2J\lambda & -2J\lambda & -4\lambda^2 \\ -2J\lambda & J^2 & 4\lambda^2 & 2J\lambda \\ -2J\lambda & 4\lambda^2 & J^2 & 2J\lambda \\ -4\lambda^2 & 2J\lambda & 2J\lambda & J^2 \end{pmatrix}. \tag{3.19}$$

We will use this matrix to characterize the two-mode squeezed state. All relevant two-

point correlators can be extracted from it. We find the average cavity photon numbers,

$$\langle \hat{a}^\dagger \hat{a} \rangle = \langle \hat{b}^\dagger \hat{b} \rangle = \frac{2\lambda^2}{J^2 - 4\lambda^2}, \quad (3.20)$$

the anomalous single-mode correlators,

$$\langle \hat{a} \hat{a} \rangle = -\langle \hat{b} \hat{b} \rangle = \frac{iJ\lambda}{J^2 - 4\lambda^2}, \quad (3.21)$$

and the two-mode correlations,

$$\langle \hat{a} \hat{b} \rangle = \frac{-J\lambda}{J^2 - 4\lambda^2}, \quad \langle \hat{a}^\dagger \hat{b} \rangle = \frac{2i\lambda^2}{J^2 - 4\lambda^2}. \quad (3.22)$$

The state exhibits single and two-mode squeezing correlations, as well as beam splitter correlations, as expected from Eq. (3.15). Note that despite the nonreciprocity, the state is symmetric between the two modes (up to an overall sign).

3.2.3 Parametric instability

As we saw in Subsec. 2.1.2, the parametric drives can render the system unstable. For our state, this threshold is obtained by looking at the denominator of the covariance matrix prefactor. Since the system will diverge if this denominator reaches zero, the threshold is given by,

$$|\lambda| \leq \frac{J}{2}. \quad (3.23)$$

Violation of this condition also corresponds to our linear system's dynamical matrix \hat{Q} having eigenvalues with nonzero real part (c.f. Appendix A), which leads to exponentially growing modes. The maximum permitted drive strength is half of the coherent tunneling magnitude.

3.2.4 Logarithmic negativity

We will now determine how useful our pure steady-state is by measuring its entanglement. The entanglement is quantified with the logarithmic negativity E_N [73]. For a system with two tensored Hilbert space components A, B, we define,

$$E_N = \log_2 (\|\rho^{(A)}\|_1), \quad (3.24)$$

where $\rho^{(A)}$ indicates the partial transpose of the density matrix with subsystem A transposed, and $\|\cdot\|_1$ is the trace norm. The logarithmic negativity is an easy-to-compute, monotone measure of entanglement for any bipartite quantum state. It can be expressed in terms of the covariance matrix via,

$$E_N = -\log_2 \left[\sqrt{2\Delta - 2\sqrt{\Delta^2 - 4\det(C)}} \right], \quad (3.25)$$

$$\Delta = \det(\alpha_c) + \det(\beta_c) - 2\det(\gamma_c),$$

where $\det(\cdot)$ is the determinant and the 2×2 matrices α_c , β_c and γ_c are the components of the covariance matrix,

$$C = \begin{pmatrix} \alpha_c & \gamma_c \\ \gamma_c^* & \beta_c \end{pmatrix}. \quad (3.26)$$

The matrix γ_c encapsulates the cross-correlations between A and B. If they grow large enough in comparison to the self-correlations, then the state becomes entangled. The logarithmic negativity is an extension of the Peres-Holodecki criterion for entanglement [74]. As an easy example, the logarithmic negativity for a pure two-mode squeezed vacuum state $\hat{S}_{ab}(\zeta) |0\rangle_A \otimes |0\rangle_B$ from Eq. (3.16) is given by $2|\zeta|/\ln(2)$.

For our system, we find the entanglement measure to be,

$$E_N = \frac{1}{\ln(4)} \ln \left(\frac{J + 2\lambda}{J - 2\lambda} \right). \quad (3.27)$$

The logarithmic negativity diverges, allowing us to make it arbitrarily high by driving close to instability. The state becomes more and more squeezed.

The logarithmic negativity for such a two-cavity cascaded system was shown by Koga & Yamamoto in an alternate context [75]. However, the approach we take here can lead us to improvements on the base setup. In the rest of this chapter, we will discuss the role that nonreciprocity actually plays in this state's generation, and show that there are cases where we can do better by deviating away from it.

3.3 Adiabatic continuity

The setup in Eq. (3.1) is a cascaded system. We either have a chiral waveguide implemented with circulators [Fig. 2.2(a)] or a synthetic reservoir with a damped auxiliary cavity [Fig. 2.2(b)]. In both of these cases, to have chirality we must match the coherent coupling and the nonlocal dissipator strength.

However, as we have seen in Subsec. 2.3.2, the synthetic implementation allows us to have $J \neq \Gamma$ [c.f. Eqs. (2.22), (2.23)]. The key point to realize is that if we do not match these two coefficients, thus breaking nonreciprocity, the perfect absorber recipe will still work.

The only role that the dissipator plays in the recipe is providing the dark-state condition in Eq. (2.25). But this condition only depends on the dissipator's jump operator, and says nothing about the prefactor. In principle, *any* dissipator strength should result in the same steady-state. The dissipator's only role is to selectively remove the unwanted excitations during the transient dynamics. Once the steady state reached, it plays no role. The J parameter in the steady state is exclusively set by the coherent coupling.

This freedom of parameter choice is a welcome relaxation of the conditions needed to make the perfect absorber recipe work. Moreover, it allows us to avoid the usage of a lossy circulator. The unwanted sources of loss in the problem would now be direct leakage from the cavities, which can be made far more robust.

However, the invariance of the steady state under changes in Γ is a manifestation of an overall property for this class of systems. Recall that for any Hamiltonian, if we vary some parameter adiabatically, the system will remain in a single eigenstate provided that this eigenstate has an energy gap to all the others. In our setup, we can consider an equivalent notion of a *dissipative* gap [43, 76]. As long as we vary our system parameters without closing this effective gap, we will remain in a unique steady-state exhibiting the same qualitative properties (such as entanglement).

To be more concrete, recall that the Lindblad master equation can be vectorized into a simple linear algebra problem (c.f. Subsec. 2.2.2). The Liouvillian acts as an effective non-Hermitian Hamiltonian. If we have a unique steady-state, it will have a single zero eigenvalue. The second-lowest magnitude eigenvalue will then act as our dissipative gap [43, 76]. Changing the prefactor Γ of the dissipator does not close this gap, and so we still have a steady-state with two-mode squeezing. Since the form of the steady-state does not contain Γ explicitly, then by analytic continuation, it remains exactly the same.

Note that since our Hamiltonian and dissipator are both quadratic, the nonvanishing nature of the dissipative gap can be confirmed just by looking at the eigenvalues of the 4×4 dynamical matrix \hat{Q} for the system (c.f. Appendix A). These are given by,

$$\nu = -\Gamma \pm \sqrt{\Gamma^2 - (J^2 - 4\lambda^2)}, \quad (3.28)$$

each twofold degenerate. We see that as long as the system obeys the stability condition from Eq. (3.23), the eigenvalues will always stay below zero, regardless of the choice of Γ . All modes will remain damped, and the Gaussian steady-state will remain unique.

We will now show another example of this ‘dissipative’ continuity. As seen in Fig. 2.2(b), our nonlocal correlated dissipator can be made with a synthetic setup using a damped auxiliary third cavity. We define this cavity to have an annihilation operator \hat{c} , and couple

it to the other two [58, 65]. Such a system would be described by,

$$\begin{aligned}\hat{H} &= \hat{H}_A + \hat{H}_B + J(\hat{a}^\dagger \hat{b} + h.c.) + G[\hat{c}^\dagger(\hat{a} - i\hat{b}) + h.c.], \\ \frac{d}{dt}\rho &= -i[\hat{H}, \rho] + \gamma\mathcal{L}[\hat{c}]\rho,\end{aligned}\tag{3.29}$$

where G is some coupling strength, and γ is the damping on the auxiliary cavity (assuming the left-to-right chirality). The Hamiltonians \hat{H}_A , \hat{H}_B are the same parametric drives as in Eq. (3.2), with equal amplitude $\lambda_A = \lambda_B = \lambda$.

If we wanted to have a chiral system, we would need to be careful about how we couple our third cavity to the first two. The system would also need to be damped hard enough to be in the Markovian limit needed for the Lindblad formulation. The equivalent dissipation strength, after tracing out cavity C, would scale as $\Gamma = 4G^2/\gamma$ [58].

However, since we do not care about what equivalent Γ we get, the couplings G can be left arbitrary. More interestingly, the damping rate γ can also be arbitrary. In fact, for *any* G , γ , we will have the same steady-state $|\psi_{\text{PD}}\rangle$.

The overall result is rather disturbing. We can get our steady-state just by attaching any cavity to our first two, as long as we damp it at least a little, and get that relative phase $\pm e^{i\pi/2}$ between them to break time-reversal symmetry. This re-delegation of the nonreciprocal dynamics to a third cavity does not close the dissipative gap for the A, B subsystem, and so our state remains the same.

Of course, a real experiment would still need to be careful about choosing these parameters. They will control the speed at which the steady-state is reached, and their amplitudes will determine how vulnerable the setup is to imperfections. In the following section, we will see how our squeezed-state generation is affected by unwanted losses.

3.4 Intrinsic loss

A realistic cavity in cQED will have some intrinsic decay rate of excitations. This leakage is unavoidable, and must be accounted for in any realistic experiment. We can model this leakage with additional terms in the master equation,

$$\frac{d}{dt}\rho = -i[\hat{H}_{\text{PD}}, \rho] + 2\Gamma\mathcal{L}[\hat{a} - i\hat{b}] + \kappa\mathcal{L}[\hat{a}]\rho + \kappa\mathcal{L}[\hat{b}]\rho. \quad (3.30)$$

Here, κ is the decay rate out of the cavities, assumed to be equal. For $\kappa > 0$, the perfect absorber recipe is no longer fulfilled, and the state will attain some impurity. The maximum entanglement is likewise no longer infinite. Fig. 3.2(a) plots the logarithmic negativity in terms of the drive strength. It now attains a maximum value for some intermediate drive strength before hitting instability, and then crashes back down.

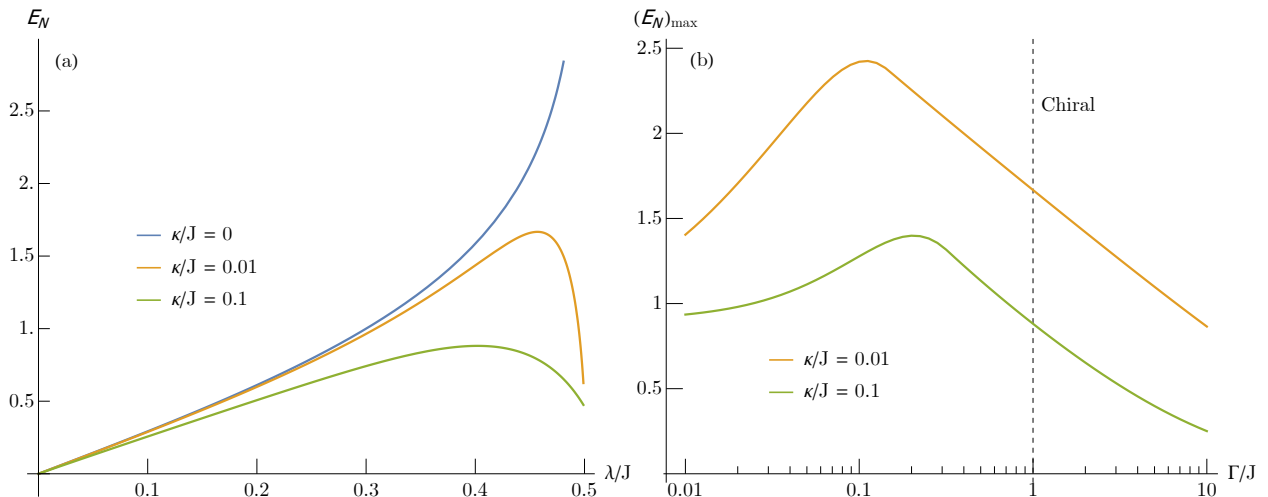


Figure 3.2: (a) Logarithmic negativity E_N of the steady-state for the parametrically-driven lossy system described in Eq. (3.30). We fix $J = 1$ and plot in terms of drive strength λ/J , up to the instability threshold. The perfect κ/J curve diverges as instability is approached. Note that the instability threshold changes slightly for $\kappa/J \neq 0$, instead becoming $\lambda < \sqrt{J^2 + 2\Gamma\kappa + \kappa^2}/2$. (b) Maximum logarithmic negativity $(E_N)_{\text{max}}$, optimized over all possible stable drives λ/J , in terms of the nonchirality ratio Γ/J . The chiral limit is marked with a dashed line.

This behaviour occurs because when we get very close to instability, the diverging photon populations will amplify the effect of the intrinsic damping terms. The engineered dissipator does not share this property because it has no effect on the ideal steady-state regardless of

population. Thus for very strong drives, unwanted loss will dominate and remove all the entanglement correlations.

This leads to a natural extension for the model. We know that having $J \neq \Gamma$ will not change the steady-state for an ideal system. However, when loss is present, this is no longer the case. As it turns out, we can have higher entanglement if we purposefully mismatch the two, thereby deviating from a cascaded system.

Fig. 3.2(b) plots the maximum logarithmic negativity in terms of Γ/J . We choose the best possible value of λ/J without going unstable. For losses on the order of $\kappa/J = 0.01$, we see close to a factor-of-two improvement by deviating away from the chiral limit. The reasoning for this is the same as mentioned before - it is the point where an optimum is found between the two entangling processes.

We have omitted the explicit forms of E_N for simplicity, as the expressions grow far more involved than the ideal case. However, for a fixed choice of drive strength the optimum choice of Γ can be approximated by,

$$\Gamma_{\text{opt}} = \sqrt{\lambda(J - 2\lambda)} + \mathcal{O}\left(\frac{\kappa}{J - 2\lambda}\right). \quad (3.31)$$

Even to zeroth order in the perturbing terms, the optimum value of Γ is much smaller than the chiral limit if the drive is close to instability.

3.5 Conclusion

We have given a simple scheme for generating states with two-mode squeezing, as described by Eq. (3.14). To get higher amounts of squeezing, we drive close to the instability threshold, and tune Γ to satisfy Eq. (3.31). The resulting pure steady-state will be $|\psi_{\text{PD}}\rangle$ from Eq. (3.12).

This scheme only uses local interactions and quadratic Hamiltonian elements, making it straightforward to realize both in cQED and other experimental platforms. It also generates two-mode squeezing with the use of just a single dissipative reservoir, in contrast to

conventional schemes that need two.

Chapter 4

Entangled cat state stabilization

The previous chapter gave an explicit system that generates entangled two-mode squeezed states. We will now extend this result to instead generate non-Gaussian entangled cat states.

As discussed in Subsec. 2.1.3, cat states have seen significant recent interest in quantum information theory [22, 23, 24, 25, 26, 27, 28]. Cat states are more robust to loss than conventional qubits, because they encode their information in an infinite-dimensional Hilbert space for which small perturbations are less damaging. Aside from qubits, entangled cat states (or equivalently entangled coherent states) have seen uses in quantum teleportation [77, 78, 79, 80], quantum repeaters [81], metrology [27, 82] and other applications detailed in Ref. [83].

Cat states are more attractive than squeezed-states for implementing qubits. Their parity provides a natural two-part structure (the even and odd cat), while still being encoded in an infinite-dimensional Hilbert space. Two-mode squeezed states do not share this property. Moreover, high entanglement in a two-mode squeezed state requires us to drive very close to instability, which greatly weakens the state's purity in the presence of loss.

To use cat states as qubits, we must be able to implement logic gates on them, which entail entangling operations between two qubits. We must thus be able to generate entangled cat-states. Few schemes exist for this purpose, both experimentally and theoretically. A recent experiment by the Yale group was able to produce entangled cats with 3D cavities

connected to a transmon and subject to pulse sequences [23]. Older theoretical proposals exist using laser pulses on finite-qubit arrays [84], trapped ions [85] or transient times in Kerr-nonlinear cavities [35]. There was a proposal using reservoir engineering via interaction with atom beams [86], but it reported difficulty due to cavity loss. In general, these proposals require significant resources, which poses a scaling challenge for quantum computers.

In this chapter, we will modify our two-cavity cascaded system by adding local self-Kerr nonlinearities to the cavities. These are fourth-order terms of the form $\hat{a}^\dagger \hat{a}^\dagger \hat{a} \hat{a}$, which can be thought of as a cavity frequency that depends on the photon number [64, 87, 9]. For a cQED implementation, a self-Kerr effect arises from including a Josephson junction in the circuit.

The resulting system will no longer be quadratic, and as such, will contain the necessary ingredients for making entangled cat states without any complicated nonlocal interactions.

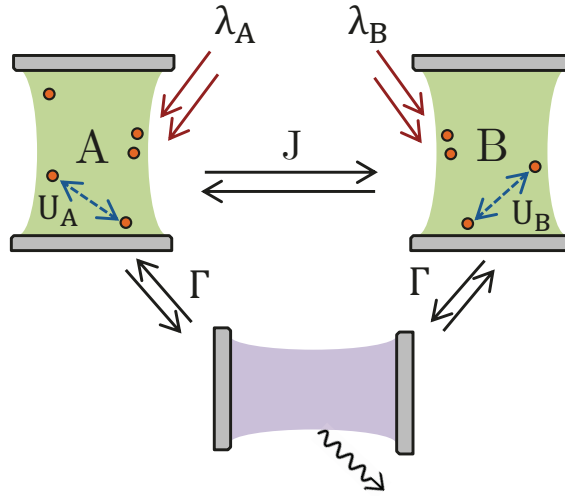


Figure 4.1: Two Kerr parametric oscillator setup from Eqs. (4.16), (4.17), assuming a synthetic waveguide implementation with an auxiliary cavity for clarity. We do not mandate the chiral limit, allowing the dissipator strength Γ and coherent coupling J to be distinct.

4.1 Single Kerr parametric oscillator

Before trying to add nonlinear interactions to a two-cavity problem, we first look to see what happens in a single-cavity parametrically driven system when a self-Kerr is present. The eventual goal is to have two, but recall that if we make things nonreciprocal, cavity A will obey an effective single-cavity master equation [c.f. Eq. (2.21)]. It will have parametric driving, self-Kerr nonlinearity, and single-photon loss,

$$\begin{aligned}\hat{H}_{\text{KPO}} &= \lambda(\hat{a}\hat{a} + h.c.) - U\hat{a}^\dagger\hat{a}^\dagger\hat{a}\hat{a}, \\ \frac{d}{dt}\rho &= -i[\hat{H}_{\text{KPO}}, \rho] + \kappa\mathcal{L}[\hat{a}]\rho.\end{aligned}\tag{4.1}$$

Here U is the strength of the nonlinearity, and κ the intrinsic loss rate. Fig. 4.2 plots a schematic. We assume that the system is driven on-resonance for now. The subscript ‘KPO’ stands for Kerr Parametric Oscillator. This system has seen much recent interest in cQED for its application to cat codes [88, 24]. For a chiral setup, it will map back to the engineered dissipator via $\kappa = 2\Gamma$.

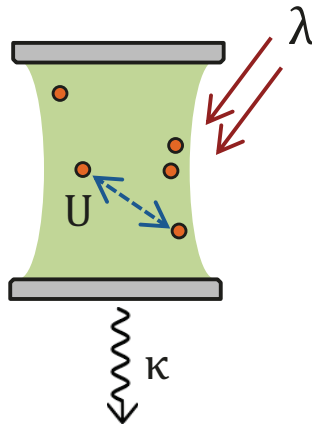


Figure 4.2: Single Kerr parametric oscillator setup from Eq. (4.1). This maps back to the reduced equations of motion for cavity A in a two-oscillator chiral setup.

A good grasp on what happens to cavity A will help with understanding the subsequent results for the more complicated two-part system.

4.1.1 Hamiltonian and eigenstates

Before considering the effects of dissipation, we note that \hat{H}_{KPO} has two degenerate eigenstates. This can be seen by rearranging the terms and acting with them on a coherent state,

$$\hat{H}_{\text{KPO}} |\alpha\rangle = \lambda\alpha^2 |\alpha\rangle + (\lambda - U\alpha^2)\hat{a}^\dagger\hat{a}^\dagger |\alpha\rangle. \quad (4.2)$$

The prefactor of the second term can be cancelled by choosing $\alpha^2 = \lambda/U$. We thus find two degenerate coherent eigenstates, with equal magnitude and opposite phase,

$$\begin{aligned} \hat{H}_{\text{KPO}} |\pm\alpha\rangle &= \frac{\lambda^2}{U} |\pm\alpha\rangle, \\ \alpha &= \sqrt{\frac{\lambda}{U}}. \end{aligned} \quad (4.3)$$

This degeneracy is only made possible by the fact that our Hamiltonian has parity symmetry. Both the drive and the Kerr nonlinearity do not mix the even and odd-parity subspaces.

Note that the two eigenstates are not completely orthogonal. Their overlap is exponentially vanishing, $\langle +\alpha | -\alpha \rangle \sim e^{-2|\alpha|^2}$, but is nonzero. We instead consider an equivalent orthogonal basis of cat states, as defined in Eq. (2.12),

$$\hat{H}_{\text{KPO}} |\mathcal{C}_\pm(\alpha)\rangle = \frac{\lambda^2}{U} |\mathcal{C}_\pm(\alpha)\rangle. \quad (4.4)$$

The presence of the nonlinearity keeps the system from going parametrically unstable, no matter how big the drive gets. The parity conservation allows the system to oscillate between a wide variety of non-Gaussian states that depend on the initial condition for the evolution. However, with no dissipation present, the system can never reach a steady-state, and will undergo coherent evolution indefinitely.

In the following subsection, we will add in a dissipative term to break the parity symmetry.

4.1.2 Damping and degenerate perturbation theory

We will now consider the effects of the intrinsic loss $\kappa\mathcal{L}[\hat{a}]$. Having any nonzero value of κ breaks the parity symmetry, because it enables jumps from the even-parity subspace to the odd one and vice-versa.

With the symmetry broken, our Hamiltonian's degeneracy is also broken. There should now be one unique steady-state of the system. We can still use the perfect-absorber recipe and trace out the second cavity, as in the previous section. Indeed, we will be doing this shortly. But before we do, it is useful to at least get an approximate understanding of what to expect. Since there were two degenerate eigenstates before, we should expect the dissipation to cause them to mix.

Since we have two degenerate eigenstates and a perturbation, we will use degenerate perturbation theory. We can certainly consider the limit of very weak dissipation where $\kappa \ll 1$. However, applying perturbation theory in this case is more involved, because our perturbation is not part of the Hamiltonian. In what follows, we will outline a superoperator equivalent of degenerate perturbation theory, and apply it to this system. There are existing results for dissipative quantum system perturbation theory [89, 90], but we will find that the simple version shown here is sufficient for our purposes.

Referring back to Subsec. 2.2.2, we re-express our master equation in terms of Liouvillian superoperators,

$$\begin{aligned} \frac{d}{dt}\rho_v &= L_0\rho_v + L_1\rho_v, \\ L_0 &= -i(\mathbb{1} \otimes \hat{H}_{\text{KPO}} - \hat{H}_{\text{KPO}}^T \otimes \mathbb{1}), \\ L_1 &= \kappa \left(\hat{a} \otimes \hat{a} - \frac{1}{2}\mathbb{1} \otimes \hat{a}^\dagger\hat{a} - \frac{1}{2}\hat{a}^\dagger\hat{a} \otimes \mathbb{1} \right). \end{aligned} \tag{4.5}$$

Recall that ρ_v is just the density matrix for the system with its columns stacked to form a supervector. This form of the master equation is almost equivalent to a Hamiltonian with a perturbation term. The supervector ρ_v plays the role of the wavefunction. The Liouvillian superoperators L_0, L_1 act as the degenerate Hamiltonian and perturbation respectively. The

key difference is that the L_j are not Hermitian.

The Liouvillian L_0 has degenerate eigenvectors that we already know, because it just corresponds to \hat{H}_{KPO} . However, since our eigenvectors now map to density matrices, we must consider all possible outer products of the Hamiltonian eigenstates in our basis. Using the two cat states in Eq. (4.4), we define,

$$\begin{aligned}
 |\phi_1\rangle\rangle &= (|\mathcal{C}_+(\alpha)\rangle \langle \mathcal{C}_+(\alpha)|)_v, \\
 |\phi_2\rangle\rangle &= (|\mathcal{C}_-(\alpha)\rangle \langle \mathcal{C}_-(\alpha)|)_v, \\
 |\phi_3\rangle\rangle &= (|\mathcal{C}_+(\alpha)\rangle \langle \mathcal{C}_-(\alpha)|)_v, \\
 |\phi_4\rangle\rangle &= (|\mathcal{C}_-(\alpha)\rangle \langle \mathcal{C}_+(\alpha)|)_v.
 \end{aligned} \tag{4.6}$$

To be clear, the double-angle bracket notation means that these are vectorized outer products, rather than wavefunctions. The first two supervectors $|\phi_1\rangle\rangle$ and $|\phi_2\rangle\rangle$ correspond to the populations of the first and second degenerate eigenstates respectively. The other two are the coherences between these two states. These states are orthonormal as required:

$$\langle\langle \phi_i | \phi_j \rangle\rangle = \delta_{ij}. \tag{4.7}$$

All four of these are also degenerate right eigenvectors of L_0 :

$$L_0 |\phi_i\rangle\rangle = 0. \tag{4.8}$$

Note that while they were not *zero-energy* eigenstates of the Hamiltonian, they do become zero-eigenvalue eigenstates of the Liouvillian, because of the subtraction in the Liouvillian's definition.

Normally, having non-Hermitian operators would mean that we have to distinguish between left and right eigenvectors. However, since our eigenbasis consists of degenerate outer products of Hamiltonian eigenstates and the Liouvillian L_0 only corresponds to coherent

Hamiltonian terms, the left and right eigenvectors coincide.

What we do now is the standard degenerate perturbation-theory approach of diagonalizing L_1 in our degenerate eigenbasis. We project it onto the four supervectors of interest¹, yielding,

$$\langle\langle\phi_i|L_1|\phi_j\rangle\rangle = \kappa\alpha^2 \begin{pmatrix} -\tanh(\alpha^2) & \coth(\alpha^2) & 0 & 0 \\ \tanh(\alpha^2) & -\coth(\alpha^2) & 0 & 0 \\ 0 & 0 & -\coth(2\alpha^2) & 1 \\ 0 & 0 & 1 & -\coth(2\alpha^2) \end{pmatrix}. \quad (4.9)$$

Keep in mind that $\alpha = \sqrt{\lambda/U}$ can be thought of as the drive strength, in units of the Kerr nonlinearity. Here, the upper 2×2 block corresponds to transitions between the system eigenstates. The lower 2×2 block corresponds to decay and coupling of system coherences to one another.

The next step is to diagonalize the matrix. We find four eigenvectors $|\psi_j\rangle\rangle$ and four eigenvalues E_j , given by,

$$\begin{aligned} E_1 &= 0, & |\psi_1\rangle\rangle &= \begin{pmatrix} \coth^2(\alpha^2) & 1 & 0 & 0 \end{pmatrix}, \\ E_2 &= -2\kappa\alpha^2 \coth(2\alpha^2), & |\psi_2\rangle\rangle &= \begin{pmatrix} 1 & -1 & 0 & 0 \end{pmatrix}, \\ E_3 &= -\frac{\kappa\alpha^2}{2} \tanh(\alpha^2) [\coth(\alpha^2) - 1]^2, & |\psi_3\rangle\rangle &= \begin{pmatrix} 0 & 0 & 1 & 1 \end{pmatrix}, \\ E_4 &= -\frac{\kappa\alpha^2}{2} \tanh(\alpha^2) [\coth(\alpha^2) + 1]^2, & |\psi_4\rangle\rangle &= \begin{pmatrix} 0 & 0 & -1 & 1 \end{pmatrix}. \end{aligned} \quad (4.10)$$

Immediately, the steady-state of the system can be identified. It corresponds to the zero-eigenvalue, $E_1 = 0$. All the other eigenstates have eigenvalues with negative real part, meaning that they represent various decay rates in the system. The form of the steady-state density matrix can be determined from $|\psi_1\rangle\rangle$. Looking back to our basis in Eq. (4.6), we can

¹While these results may be proven rigorously, it can be easier to just compute the projections for small finite Hilbert space sizes N , interpolate the $N \rightarrow \infty$ limit and verify it with numerics.

un-vectorize it to recover,

$$\rho_{\text{st}} = \mathcal{N} [\coth^2(\alpha^2) |\mathcal{C}_+(\alpha)\rangle \langle \mathcal{C}_+(\alpha)| + |\mathcal{C}_-(\alpha)\rangle \langle \mathcal{C}_-(\alpha)|], \quad (4.11)$$

where \mathcal{N} is a normalization constant. Our steady-state is an incoherent mixture of even and odd cat states, with some bias towards the even cat that grows weaker as the drive strength increases. This bias can be explained by the fact that for low drive strengths, the steady-state is the vacuum, which has even parity. If we instead assume that the drive is very strong, i.e. $\alpha \gg 1$, we have $\coth(\alpha^2) \approx 1$ and the steady-state can be rewritten back in terms of coherent states:

$$\rho_{\text{st}} = \mathcal{N} (|\alpha\rangle \langle \alpha| + |-\alpha\rangle \langle -\alpha|) + \mathcal{O}(e^{-2\alpha^2}). \quad (4.12)$$

Thus our steady state is just an equal mixture of the $|\pm\alpha\rangle$ coherent eigenstates from our original Hamiltonian. The effect of the dissipation to zeroth order is to induce jumps between them, which will stabilize in the long-time limit until both states have the same population. This steady-state for a Kerr parametric oscillator is in line with recent results from Refs. [88, 24].

While all these calculations have assumed a negative Kerr nonlinearity, having a positive one yields almost the same result. The only thing that changes is the phase of the coherent eigenstates, which would become $|\pm i\alpha\rangle$ instead. Their corresponding Hamiltonian eigenvalues would change accordingly to $\hat{H}_{\text{KPO}} |\pm i\alpha\rangle = -\lambda^2/U |\pm i\alpha\rangle$. All of the rates in Eq. (4.10) would otherwise remain the same.

4.1.3 Slow rates

The degenerate perturbation theory in the previous subsection gave us the approximate form of the Kerr parametric oscillator's steady-state. However, it can also tell us something about the transient rates in the system. After all, the projected matrix L_1 has four eigenvalues,

each of them describing a certain kind of decay that the dissipation induces.

Eigenvalue E_3 is of particular interest. If we are assuming a strong drive $\alpha \gg 1$, then the magnitude of the eigenvalue gets very small because of the $[\coth(\alpha^2) - 1]^2$ term:

$$E_3 = 2\kappa\alpha^2 e^{-4\alpha^2} + \mathcal{O}\left(e^{-6\alpha^2}\right). \quad (4.13)$$

This eigenvalue is the approximate dissipative gap for the system.

The eigenvector corresponding to E_3 may be rewritten in terms of the original coherent eigenstates of the Hamiltonian,

$$|\phi_3\rangle\rangle = (|\alpha\rangle\langle\alpha| - |-\alpha\rangle\langle-\alpha|)_v. \quad (4.14)$$

Note that this eigenvector does not have to correspond to a valid density matrix, because it describes a rate and not a steady-state. The eigenvector describes the transfer of population from $|\alpha\rangle$ to $|-\alpha\rangle$, and vice-versa. Any system with an initial state biased towards one of the two coherent eigenstates will have to be equalized by this slow rate.

Fig. 4.3 plots a numerically-computed dissipative gap E_{slow} in terms of the drive strength, comparing it to our theoretical prediction of E_3 . The numerics are worked out by finding the smallest-magnitude nonzero eigenvalue of the full Liouvillian in the Fock basis. Our approximation for the slow rate magnitude holds until the drive strength gets too large. This is to be expected, as our perturbation is proportional to $\kappa\alpha^2$. If α gets large enough, i.e. $\kappa\alpha^2 \geq U$, higher-order processes will kick in and first-order degenerate perturbation theory will no longer be sufficient.

The inset of Fig. 4.3 plots the fidelity of the numerically-obtained slow rate eigenvector with our exact prediction of $|\phi_3\rangle\rangle$. The fidelity is defined by,

$$F = \left| \text{tr} \left(\sqrt{\sqrt{\rho_1}\rho_2\sqrt{\rho_1}} \right) \right|^2, \quad (4.15)$$

where ρ_1 and ρ_2 are the un-stacked supervectors². We see that $F > 0.999$ for all sampled points. Unlike the eigenvalue comparisons, the fidelity increases with the drive monotonically. This means that while our approximations for the slow rate itself will cease to hold for $\kappa\alpha^2 \gg 1$, the process that the slow rate describes will always be the simple population decay in Eq. (4.14).

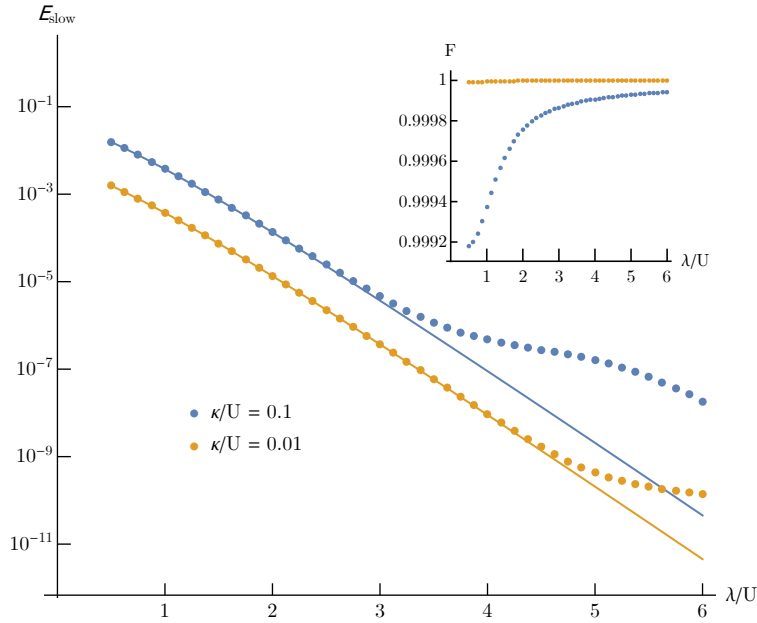


Figure 4.3: Slowest decay rate of the damped single Kerr parametric oscillator system, in terms of the drive strength λ/U . The points are obtained by numerically finding the smallest-magnitude nonzero eigenvalue of the full Liouvillian, using a truncated Hilbert space size of $N=50$ Fock states. The solid lines are the theoretical predictions from degenerate perturbation theory, given by E_3 in Eq. (4.10). The inset computes the fidelity between the numerically obtained eigenvector and the predicted population decay $|\phi_3\rangle$ from Eq. (4.14).

We can explicitly see the effect of the slow rate in Fig. 4.4, which plots the fidelity of the numerically-obtained density matrix with the steady-state form in Eq. (4.12). Starting from a vacuum state, which has equal overlap with both coherent eigenstates, allows one to reach the steady-state quickly. On the other hand, beginning entirely in one of the two eigenstates causes significant metastability, as observed in Refs. [88, 24]. The system has to move half of its population from one coherent eigenstate to the other, which is constrained by the slow

²For a supervector of the Liouvillian with nonzero eigenvalue, we can also get away with taking a simple inner product instead. However, if the supervector corresponds to a density matrix, this is not permitted because the normalizations are not equivalent. If ρ is a density matrix corresponding to an impure state, then $\|\rho\|_1 \neq \|\rho_v\|$.

rate E_3 and takes a long time.

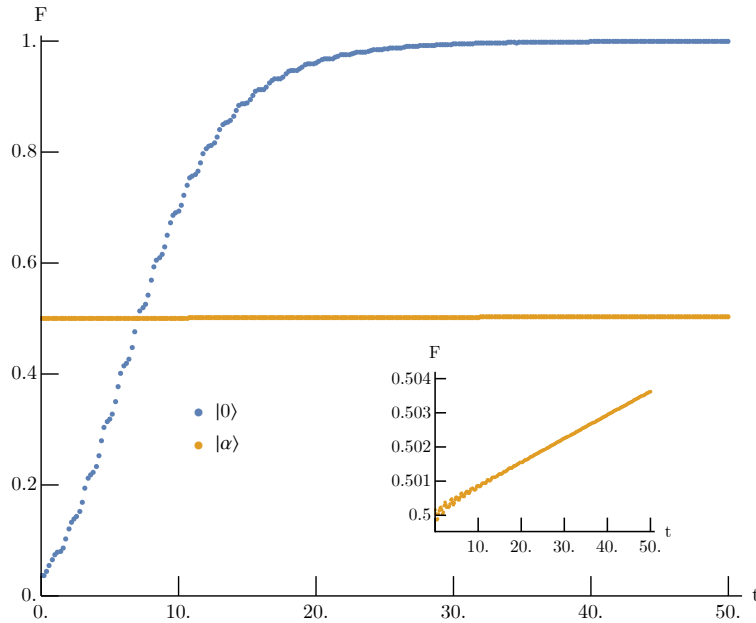


Figure 4.4: Time evolution of the single Kerr parametric oscillator state fidelity with our theoretical prediction in Eq. (4.12). We choose parameters of $\lambda/U = 2$ and $\kappa/U = 0.1$. The blue dots correspond to evolution from a vacuum state initial condition, $|\psi_0\rangle = |0\rangle$. The orange dots have the system initialized in one of the two coherent eigenstates, $|\psi_0\rangle = |\alpha\rangle$ with $\alpha = \sqrt{\lambda/U}$. The inset plots the fidelity of just the second initial condition, showing the slow near-linear growth. Applying linear regression to the second half of the points in the inset yields an approximate linear slope of $E_{\text{slow}} \approx 1.38 \times 10^{-4}$ (accounting for a factor of two coming from the exponent in the definition of F). The predicted value to compare against is $E_3/2 = 1.34 \times 10^{-4}$. The Hilbert space for these simulations is constrained to $N = 25$ Fock states.

The overall conclusions to make about the single KPO are twofold. We see that it has a degenerate subspace of cat eigenstates, which naturally implies that having two KPOs will allow us to entangle the cats. This will be shown in the next section. However, we must also be very careful with our initial conditions and parametric regimes. If we want to reach the steady-state of the system quickly, we must avoid a starting point that is biased towards one of the two degenerate eigenstates. Furthermore, if there are additional sources of error or imperfections in the model with magnitude exceeding the dissipative gap, they can overpower the fragile population decay and change the steady-state.

4.2 Two-cavity Kerr perfect absorber

Now that the dynamics for a single KPO have been worked out, we return to our original goal of a two-cavity system. We add a second KPO, and couple it to the first with simple single-photon tunneling and engineered dissipation.

The system that we are looking at is analogous to the non-Kerr system in Sec. 3.1, with the only difference being the addition of self-Kerr nonlinearities to both cavities. Putting a Kerr nonlinearity on cavity B is also motivated by the perfect absorber recipe, which works by mimicking the terms in first cavity.

Following the perfect absorber recipe, we write a general form for the Hamiltonian,

$$\begin{aligned}
\hat{H}_{\text{EC}} &= \hat{H}_{\text{A}} + \hat{H}_{\text{B}} + J(\hat{a}^\dagger \hat{b} + h.c.), \\
\hat{H}_{\text{A}} &= \lambda_{\text{A}}(\hat{a}\hat{a} + h.c.) + U_{\text{A}}\hat{a}^\dagger \hat{a}^\dagger \hat{a}\hat{a}, \\
\hat{H}_{\text{B}} &= \lambda_{\text{B}}(e^{i\phi}\hat{b}\hat{b} + h.c.) + U_{\text{B}}\hat{b}^\dagger \hat{b}^\dagger \hat{b}\hat{b}.
\end{aligned} \tag{4.16}$$

The master equation obeyed by the system is given by,

$$\frac{d}{dt}\rho = -i[\hat{H}_{\text{EC}}, \rho] + 2\Gamma\mathcal{L}[\hat{a} - i\hat{b}]\rho. \tag{4.17}$$

Fig. 4.1 shows a schematic of the system. Note that we have not assumed that the system is connected by a true chiral waveguide, which would correspond to $J = \Gamma$, instead considering a synthetic implementation. The amplitudes of the drives, the Kerr nonlinearities, and the phase ϕ are all parameters that we are free to tune.

We again transform to the \hat{c}_\pm basis from Eq. (3.3). The resulting Hamiltonian is,

$$\begin{aligned}
\hat{H}_{\text{EC}} &= -iJ(\hat{c}_+^\dagger \hat{c}_- - h.c.) + \frac{1}{2} [(\lambda_{\text{A}} - e^{i\phi}\lambda_{\text{B}})(\hat{c}_+ \hat{c}_+ + \hat{c}_- \hat{c}_-) + h.c.] + [(\lambda_{\text{A}} + e^{i\phi}\lambda_{\text{B}})\hat{c}_+ \hat{c}_- + h.c.] \\
&+ \frac{1}{4}(U_{\text{A}} + U_{\text{B}}) [\hat{c}_+^\dagger \hat{c}_+^\dagger (\hat{c}_+ \hat{c}_+ + \hat{c}_- \hat{c}_-) + h.c.] + \frac{1}{2}(U_{\text{A}} - U_{\text{B}}) [\hat{c}_+^\dagger \hat{c}_-^\dagger (\hat{c}_+ \hat{c}_+ + \hat{c}_- \hat{c}_-) + h.c.] \\
&+ (U_{\text{A}} + U_{\text{B}})\hat{c}_+^\dagger \hat{c}_-^\dagger \hat{c}_+ \hat{c}_-.
\end{aligned} \tag{4.18}$$

The first line is the same as what we saw in Eq. (3.6). The second and third lines come from throwing the Kerr nonlinearities into the mix. Their effect is to add additional effective parametric driving and cavity frequency terms, modulated by the populations of the cavities. Recall also that in this basis, the jump operator is just $\Gamma\mathcal{L}[\hat{c}_+]$.

The next step is to act with this Hamiltonian on a dark-state ansatz. Since we have the same kind of dissipator, we can still use the ansatz in Eq. (3.4). The result is,

$$\begin{aligned} \hat{H}_{\text{EC}}|\psi\rangle &= |0\rangle_+ \otimes \sum_{n=0}^{\infty} \frac{\alpha_n}{2} \left[(\lambda_A - e^{i\phi}\lambda_B)\sqrt{n(n-1)}|n-2\rangle_- + (\lambda_A - e^{-i\phi}\lambda_B)\sqrt{(n+1)(n+2)}|n+2\rangle_- \right] \\ &+ |1\rangle_+ \otimes \sum_{n=0}^{\infty} \alpha_n \left[-iJ\sqrt{n}|n-1\rangle_- + (\lambda_A + e^{-i\phi}\lambda_B)\sqrt{n+1}|n+1\rangle_- + \frac{1}{2}(U_A - U_B)\sqrt{n(n-1)}|n-1\rangle_- \right] \\ &+ |2\rangle_+ \otimes \sum_{n=0}^{\infty} \frac{\alpha_n}{\sqrt{2}} \left[(\lambda_A - e^{i\phi}\lambda_B)|n\rangle_- + \frac{1}{2}(U_A + U_B)\sqrt{n(n-1)}|n-2\rangle_- \right]. \end{aligned} \quad (4.19)$$

What we have to do is find parameters that make this resulting state an eigenstate. For the non-Kerr system, we cancelled out everything except the $|1\rangle_+$ proportional term with parameter choices, and then found coefficients α_n which yielded a zero-energy eigenstate. After some careful observation, we note that we must take the same analytical approach here.

The $|1\rangle_+$ term cannot be cancelled parametrically, because of the J -proportional term (the only other term with the same \hat{c}_- Fock state is proportional to n , and thus cannot cancel a constant). This means that we must again cancel it with a recursion relation that restricts the α_n . On the other hand, the $|0\rangle_+$ and $|2\rangle_+$ may be removed with a parameter choice of,

$$\phi = 0, \quad \lambda_A = \lambda_B = \lambda, \quad U_A = -U_B = U. \quad (4.20)$$

This is the same as in Eq. (3.8), but with the additional restriction of tuning the Kerr nonlinearities to be equal and opposite in magnitude. Having a self-Kerr interaction with a positive amplitude can still be implemented with a Josephson junction if we reverse the bias.

The resulting action of the Hamiltonian on the ansatz then simplifies down to,

$$\hat{H}_{\text{EC}} |\psi\rangle = |1\rangle_+ \otimes \sum_{n=0}^{\infty} \alpha_n [-iJ\sqrt{n} |n-1\rangle_- + 2\lambda\sqrt{n+1} |n+1\rangle_- + U\sqrt{n}(n-1) |n-1\rangle_-] = 0. \quad (4.21)$$

The coefficients for a zero-energy eigenstate may be found by solving the recursion relation,

$$\alpha_{n+1} = \frac{2\lambda}{iJ - Un} \sqrt{\frac{n}{n+1}} \alpha_{n-1}. \quad (4.22)$$

The even coefficients have an exact solution given by,

$$\alpha_{2n} = \left(\frac{-\lambda}{U}\right)^n \sqrt{\frac{(2n-1)!!}{(2n)!!}} \frac{\Gamma_g\left(\frac{1}{2} - \frac{iJ}{2U}\right)}{\Gamma_g\left(n + \frac{1}{2} - \frac{iJ}{2U}\right)} \alpha_0, \quad (4.23)$$

where \mathcal{N}_e is a normalization constant, and $\Gamma_g(\cdot)$ is the Gamma function.

As we saw before, the odd coefficients do not have an analogous exact solution because the $|0\rangle_-$ term cannot be cancelled. Thus the unique steady-state for the system with our chosen parameters is given by,

$$|\psi_e\rangle = \mathcal{N}_e |0\rangle_+ \otimes \sum_{n=0}^{\infty} \left(\frac{-\lambda}{U}\right)^n \sqrt{\frac{(2n-1)!!}{(2n)!!}} \frac{\Gamma_g\left(\frac{1}{2} - \frac{iJ}{2U}\right)}{\Gamma_g\left(n + \frac{1}{2} - \frac{iJ}{2U}\right)} |2n\rangle_-, \quad (4.24)$$

We can take the limit of $U \rightarrow 0$ to recover the result from Eq. (3.12).

Ignoring the trailing orphaned term, the odd-parity solution can also be written,

$$|\psi_o\rangle = \mathcal{N}_o |0\rangle_+ \otimes \sum_{n=0}^{\infty} \left(\frac{-\lambda}{U}\right)^n \sqrt{\frac{(2n)!!}{(2n+1)!!}} \frac{\Gamma_g\left(1 - \frac{iJ}{2U}\right)}{\Gamma_g\left(n + 1 - \frac{iJ}{2U}\right)} |2n+1\rangle_-. \quad (4.25)$$

While this is a dark-state of the dissipator, it is not a perfect eigenstate of the Hamiltonian.

Acting on it with \hat{H} gives,

$$\hat{H} |\psi_o\rangle = -iJ\mathcal{N}_o |1\rangle_+ \otimes |0\rangle_-. \quad (4.26)$$

This trailing term would normally prevent $|\psi_o\rangle$ from being a steady-state of the system.

However, we note that if the drive amplitude becomes very strong compared to the other scales in the system, the system normalization constant will grow very small, $\mathcal{N}_o \ll 1$. This means that while the odd-parity solution is never going to be an exact zero-energy eigenstate, it can get close to being one. This second state remains relevant to the dynamics, and plays a key role in the slow decay rates of the system.

4.3 Cat state properties

Now that we have the exact form of the system steady-state, we can figure out what it actually represents. The quotient of Gamma functions means that it is no longer a simple squeezed state. The non-Kerr model only had one dimensionless parameter quantifying the steady-state, which was the drive strength λ/J . In contrast, the Kerr system is characterized by two dimensionless parameters - the drive strength λ/U and the coherent coupling J/U . We choose to work in units of the Kerr nonlinearity, because the other parameters already appear this way in the steady-state coefficients.

To get a qualitative understanding of what our two dimensionless parameters do, we can look at the state Wigner function. Fig. 4.5 shows the Wigner function of the \hat{c}_- component in terms of J/U , for a fixed value of λ/U . We see that for $\lambda/J \ll 1$, the system is well-described by a squeezed state. If $\lambda/J \gg 1$, then \hat{c}_- is in a cat state instead. A smooth crossover occurs between the two regimes.

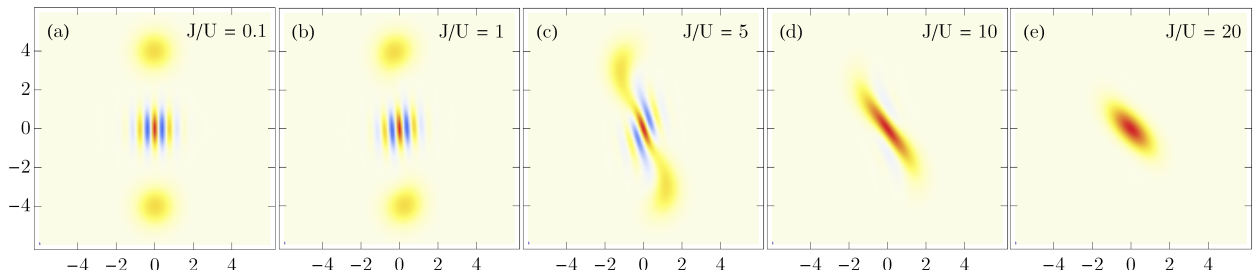


Figure 4.5: Wigner function of the \hat{c}_- steady-state $|\psi_e\rangle$ in Eq. (4.24). The drive strength is fixed at $\lambda/U = 4$. Five different values of the coherent coupling J/U are chosen, ranging from much smaller to much larger than λ/U .

The emergence of a squeezed state in the $\lambda/J \ll 1$ limit should not be surprising. If we look back at the form of the recursion relation in Eq. (4.22), the role of U is to modulate the coupling strength J by adding a photon number-dependent imaginary part to it. In a sense, the Kerr nonlinearities help keep the system stable. If J is much stronger than λ , then it alone can keep the system stable without the help of the nonlinearity. In that limit, the Kerr essentially contributes nothing to the system, and we get a state very similar to what is described by Eq. (3.12).

For $\lambda/J \gg 1$, the system can no longer be described by squeezed states because it would be unstable without the Kerr (recall that the instability threshold in the non-Kerr system is $\lambda < J/2$). The Kerr nonlinearity now plays a big role in keeping the system stable. Since it has an inherent parity symmetry, the resulting system states will also inherit these parity properties. As a result, we get the expected non-Gaussian cat state instead.

In the limit of strong drive $\lambda/J \gg 1$, the steady-state $|\psi_e\rangle$ is an even cat state in the \hat{c}_- mode. Based on our observations from the single Kerr parametric oscillator, we can expect its amplitude to scale with $\sqrt{\lambda/U}$. For practical considerations, we will also be assuming that $\lambda/U \gg 1$, so that the cat has distinguishable interference fringes in its quasiprobability distribution. It is also evident that the near-steady state $|\psi_o\rangle$ will map to an odd cat instead.

All of the observations thus far have been qualitative. To make things more concrete, we compute the fidelity of the exact Fock-basis state with a cat and squeezed state. Based on numerics, we find that the actual cat state to compare against is $|\mathcal{C}_+(i\sqrt{2\lambda/U})\rangle$. The factor of two arises from the fact that the c_- mode is enclosing the nontrivial dynamics of two Kerr parametric oscillators rather than just one. The squeezed state to compare against is the non-Kerr result from Eq. (3.12).

Fig. 4.6 plots the fidelity with these two guesses in terms of the coherent coupling strength. Note that for the cat, instead of assuming an overall phase $e^{i\pi/2}$ for the cat amplitude α , we optimize over all possible phases. This is because the cat will rotate in phase-space as J/U increases, destroying the apparent fidelity without diminishing its non-Gaussian properties.

We find the two expected regimes, going from a cat state for low coupling to a squeezed state for high coupling. The crossover occurs around $\lambda/J \approx 1/2$. We can still make J on the same order as λ , as long as the latter is bigger, and have a cat state with high fidelity. This will be useful once we begin to consider imperfections in the system, as having a higher J will help with resilience.

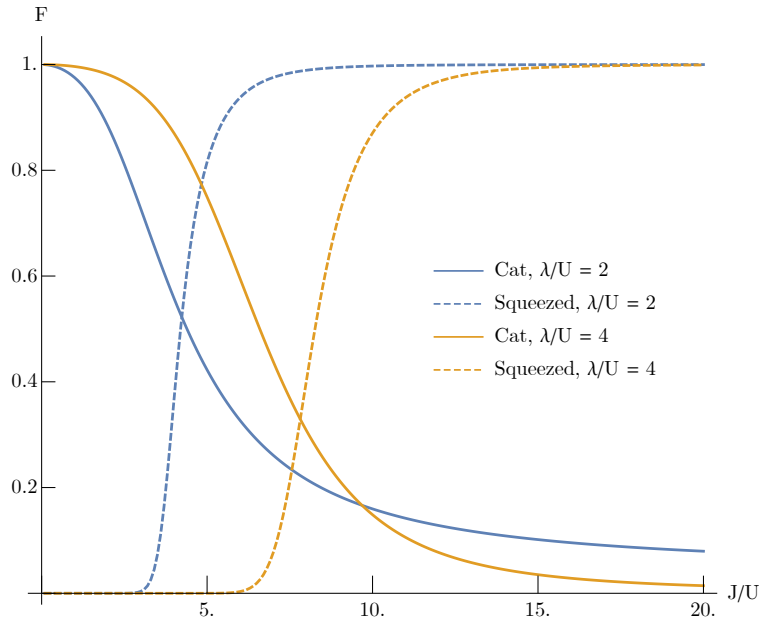


Figure 4.6: Fidelity comparison of the \hat{c}_- mode exact steady-state $|\psi_e\rangle$. The dashed lines compare with a squeezed state in Eq. (3.12). The solid lines compare to a cat state given by $|\mathcal{C}_+(e^{i\phi}\sqrt{2\lambda/U})\rangle$, optimizing over all possible angles ϕ .

4.4 Steady-state in cavity mode basis

Returning to the original cavity mode basis \hat{a}, \hat{b} is equivalent to a beam-splitter operation. The single-mode cat state of \hat{c}_- will be converted into an entangled cat state [91].

To make this explicit, we first rewrite the exact states in Eqs. (4.24),(4.25) in the \hat{a}, \hat{b}

basis,

$$\begin{aligned}
|\psi_e\rangle &= \mathcal{N}_e \sum_{\substack{n,m=0 \\ (n+m)\%2=0}}^{\infty} \left(\frac{-\lambda}{2U}\right)^{(n+m)/2} (-i)^m \sqrt{\frac{(n+m-1)!! (n+m)!}{(n+m)!! n!m!}} \frac{\Gamma\left(\frac{1}{2} - \frac{iJ}{2U}\right)}{\Gamma\left(\frac{n+m}{2} + \frac{1}{2} - \frac{iJ}{2U}\right)} |n, m\rangle, \\
|\psi_o\rangle &= \mathcal{N}_o \sum_{\substack{n,m=0 \\ (n+m)\%2=1}}^{\infty} \left(\frac{-\lambda}{2U}\right)^{(n+m)/2} (-i)^m \sqrt{\frac{(n+m-1)!! (n+m)!}{(n+m)!! n!m!}} \frac{\Gamma\left(1 - \frac{iJ}{2U}\right)}{\Gamma\left(\frac{n+m}{2} + \frac{1}{2} - \frac{iJ}{2U}\right)} |n, m\rangle.
\end{aligned} \tag{4.27}$$

Note the constraint on the double sum, which preserves the overall parity of the states. The notation $z \% 2$ means z modulo 2.

Surprisingly, one can analytically solve for the steady state of the dissipative single-cavity Kerr parametric oscillator using a technique where you use the positive P-function to convert the master equation into something that looks like a classical Fokker-Plank equation (with twice the number of degrees of freedom) [24]. After a tedious set of integrations, one can obtain the steady-state density matrix in the Fock basis. Eq. (4.27) gives a much simpler way of obtaining this solution: one just traces out cavity B to get the steady state of A. We have explicitly confirmed that this reproduces the answer obtained from (the much more complicated) positive P function approach.

Going back to the two-cavity dynamics, in the strong-driving limit, the exact states $|\psi_e\rangle$, $|\psi_o\rangle$ are approximated by entangled cats, as evidenced by rewriting the single \hat{c}_- mode cat $|\mathcal{C}_+(i\sqrt{2}\alpha)\rangle$ in the \hat{a} , \hat{b} basis. They take the form of,

$$\begin{aligned}
|\psi_e\rangle &\approx \frac{1}{\sqrt{2}} (|\mathcal{C}_+(i\alpha)\rangle \otimes |\mathcal{C}_+(\alpha)\rangle + |\mathcal{C}_-(i\alpha)\rangle \otimes |\mathcal{C}_-(\alpha)\rangle) \\
|\psi_o\rangle &\approx \frac{1}{\sqrt{2}} (|\mathcal{C}_+(i\alpha)\rangle \otimes |\mathcal{C}_-(\alpha)\rangle + |\mathcal{C}_-(i\alpha)\rangle \otimes |\mathcal{C}_+(\alpha)\rangle).
\end{aligned} \tag{4.28}$$

Recall that the cat states are defined in Eq. (2.12). Equivalently, these can be approximated

by entangled coherent states [83],

$$\begin{aligned} |\psi_e\rangle &\approx \frac{1}{\sqrt{2}} (|i\alpha\rangle \otimes |\alpha\rangle + |-i\alpha\rangle \otimes |-\alpha\rangle) \\ |\psi_o\rangle &\approx \frac{1}{\sqrt{2}} (|i\alpha\rangle \otimes |\alpha\rangle - |-i\alpha\rangle \otimes |-\alpha\rangle). \end{aligned} \tag{4.29}$$

As usual, $\alpha = \sqrt{\lambda/U}$. Note that the phase factor in the cavity A cats comes from it having a positive Kerr amplitude, as discussed at the end of Subsec. 4.1.2. These approximations hold for $\lambda/J \gg 1$.

If our system is allowed to evolve to its steady-state assuming the above approximations, we will reach a unique and pure entangled cat state. Being able to generate such a state is already a powerful result in its own right. What makes this approach far more useful, however, is that it only requires local drives and nonlinearities to accomplish. We only use one linear engineered dissipator. In contrast, recent experiments connect the cavities to a shared nonlinear transmon qubit, and have to include nonlinear two-photon dissipation [23].

Before we go on, the cat amplitude α merits some discussion. Recall that we need $\alpha = \sqrt{\lambda/U} \geq 1$ to distinguish a cat from a Gaussian vacuum or squeezed state. A cat with vanishingly small amplitude still maintains its parity structure, but most of the state population will just sit in the vacuum $|0\rangle$ and render parity discussions irrelevant. There is no firm metric for how non-Gaussian a state can be. One could deem a cat to be wide enough if there are visible interference fringes with negative values in the Wigner function for the state (we could either consider the \hat{c}_- mode, or look at the two-mode Wigner function [23]). However, these negative values can persist for small amplitudes $\alpha \approx 1$ for which the characteristic lobe structure is no longer present. The experimental results in Ref. [23] considered cats with amplitude $\alpha \approx 1.92$. If all we want is a lobe structure with visible interference fringes, however, we can go even lower to $\alpha \approx 1.5$ (i.e. $\lambda/U \approx 2$).

The reason that we want α to not be too large is the slow rates in the system. We saw in the one cavity case that the system exhibits metastability, and the decay *rate* out of this

metastability is exponential in α (meaning that the decay *time* is superexponential). Thus if α is too large, we will be unable to reach the steady-state we want in a reasonable time frame. In Sec. 4.6, we will get an analytic handle on how the slow rates in this two-cavity system affect the dynamics.

4.5 Alternate detuning implementation

Before we move on to more details of the cat-generating system, we will again bring up the adiabatic continuity from Sec. 3.3. The main argument was that our steady-state will qualitatively remain the same up to analytic continuation of any varied parameters, as long as the dissipative gap does not close.

We can see this phenomenon in action for the Kerr system's exact solution. At any point in the derivation, we can take $U \rightarrow 0$ and recover the squeezed-state generating system. The only time that this fails is if our other parameters λ, J would fall in the unstable regime for the quadratic model. This can be summarized in Fig. 4.7(a). The line with $U = 0$ and unstable $\lambda \geq J/2$ is highlighted in red. An analytic continuation from a cat state with $U \neq 0$ to a squeezed-state is shown with a blue curve. Having red means that either the gap opens to permit multiple steady-states, or the steady-state becomes parametrically unstable.

This analytic continuity is important because it can be used to include additional quadratic terms in our Hamiltonian without significant change in the steady-state. More specifically, we can include *local* terms that will replace the coherent tunnel coupling between the cavities.

Recall that our KPOs are driven on-resonance, with no effective cavity frequency terms. If we assume that this is no longer the case, then we will have detunings of the form,

$$\hat{H}_\delta = \delta_A \hat{a}^\dagger \hat{a} + \delta_B \hat{b}^\dagger \hat{b}. \quad (4.30)$$

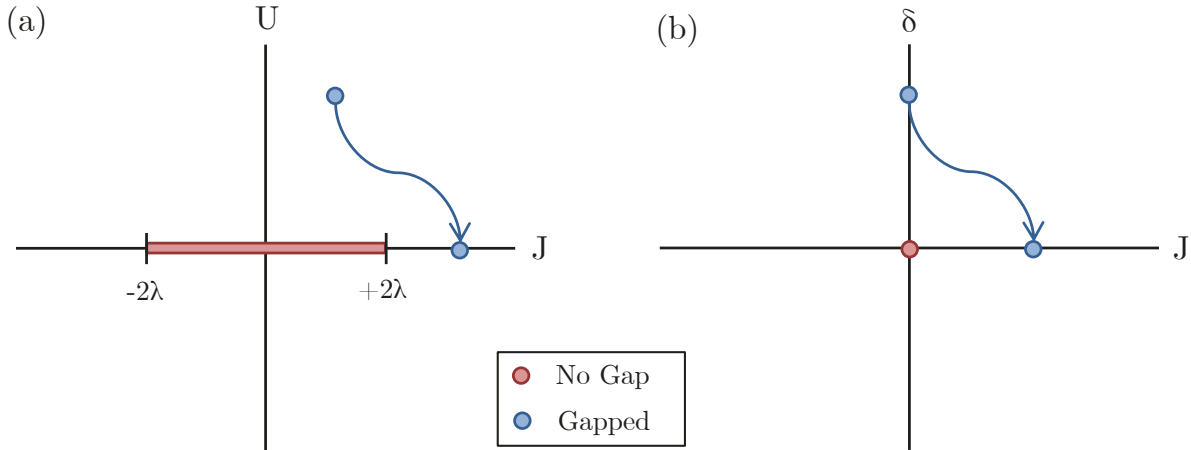


Figure 4.7: (a) Schematic diagram of the parameter space for the Kerr cat-generating model. The line with no dissipative gap, indicating instability or multiple steady-states, is highlighted in red. Gapped parameter choices are in blue. The curved line shows an analytic continuation from a squeezed cat state ($U, J \neq 0$) to a squeezed state ($U = 0$). (b) Schematic diagram between coherent coupling J and detuning δ terms, functioning as the same parameter up to a phase of $e^{-i\pi/2}$. The blue line shows an analytic continuation from a system with no broken time-reversal symmetry, to one with maximal broken time-reversal symmetry. Note that this diagram assumes $U \neq 0$, as otherwise there would be a circle of radius 2λ centered at the origin for which the system would be unstable.

In the \hat{c}_{\pm} basis, these take the form of,

$$\hat{H}_{\delta} = \frac{1}{2} (\delta_A + \delta_B) (\hat{c}_+^{\dagger} \hat{c}_+ + \hat{c}_-^{\dagger} \hat{c}_-) + \frac{1}{2} (\delta_A - \delta_B) (\hat{c}_+^{\dagger} \hat{c}_- + h.c.). \quad (4.31)$$

The key thing to notice is that the second term looks exactly like the J -proportional one in Eq. (4.18). If we now choose,

$$\delta_A = -\delta_B = \delta, \quad (4.32)$$

then the effective onsite detunings vanish and we recover the exact same Hamiltonian term as the coherent coupling. The parameter J is replaced by $i\delta$. By the same analytic continuation argument, since the gap does not vanish, the steady-state will still be $|\psi_e\rangle$ from Eq. (4.24). Fig. 4.7 showcases this transition. Assuming $U \neq 0$, the system will remain gapped and stable as long as we have either δ or J nonzero (or a combination of the two).

It is worth noting just how bizarre this outcome is. We have replaced a nonlocal term

coupling the two cavities with local detunings. The only resulting difference was that the effective coupling strength became imaginary. Generating detunings with equal-and-opposite magnitude is easier to accomplish experimentally, because we just have to drive one of the cavities at a higher pump frequency.

More importantly, this alternate detuning-based approach no longer needs to break time-reversal symmetry. Our master equation still needs a dissipator of $\mathcal{L}[\hat{a} - i\hat{b}]$. However, we can now gauge away that phase by taking $\hat{b} \rightarrow i\hat{b}$. Since there is no longer a coherent coupling, it will not ‘pick up’ this extra phase. The cavity detuning and Kerr nonlinearity are also phase-invariant. The sign of the parametric drive will change, but it will remain real-valued.

Our system will now look like,

$$\begin{aligned}\hat{H}_{\text{ECD}} &= \hat{H}_1 - \hat{H}_2, \\ \hat{H}_j &= \delta \hat{a}_j^\dagger \hat{a}_j + \lambda(\hat{a}_j \hat{a}_j + h.c.) + U \hat{a}_j^\dagger \hat{a}_j^\dagger \hat{a}_j \hat{a}_j, \\ \frac{d}{dt} \rho &= -i[\hat{H}_{\text{ECD}}, \rho] + 2\Gamma \mathcal{L}[\hat{a} + \hat{b}] \rho,\end{aligned}\tag{4.33}$$

with $\hat{a}_1 = \hat{a}$, $\hat{a}_2 = i\hat{b}$.

This offers several insights into the perfect-absorber recipe. Thanks to these adiabatic continuity arguments, we have shown that you can not only deviate from chirality, but you can also maintain time-reversal symmetry.

In what follows, we will continue using the coherent tunnel coupling between the cavities to remain in line with the literature. The detuning-based setup remains a more simple and straightforward way of implementing the design in practice. In the limit of $\delta/U \ll 1$ it qualitatively yields almost the same state, with the main difference being that δ pushes us from the cat to the squeezed state roughly twice as fast (i.e. we get the same fidelity with a cat for $J \approx 2\delta$). There is also no unwanted phase rotation, because the corresponding squeezed state has its squeezed quadrature aligned with the direction of the cat.

4.6 System imperfections

4.6.1 Slow rates

We will now characterize the effect of unwanted losses on our system. In general, the worst-case tolerance of our system to loss is set by the dissipative gap. A small gap corresponds to a slow rate, which leads to long stabilization time for the steady-state. This gives unwanted losses more time to corrupt the evolution. In the single KPO case, there was one slow rate of the Liouvillian that acted as the dissipative gap. Since our setup can map to a cascaded system under a certain choice of parameters, for which cavity A exhibits the same reduced dynamics, we expect the same rate here. However, repeating the same degenerate perturbation theory argument shows that there are now several other slow rates in the problem.

The explicit derivation can be found in Appendix C, which we omit here for brevity. Essentially, the single KPO used a basis of two cat states $|\mathcal{C}_\pm(\alpha)\rangle$, corresponding to four possible outer products. It then took the intrinsic dissipation $\mathcal{L}[\hat{a}]$ as the perturbing Liouvillian.

What we will do for two cavities is take all possible tensor products of these cat states for both cavities. This results in four states, and thus sixteen outer products to use in the perturbation theory. The unperturbed part will be the two Hamiltonians $\hat{H}_A + \hat{H}_B$. The perturbation will be the coherent coupling $J(\hat{a}^\dagger\hat{b} + h.c.)$ and engineered dissipator $2J\mathcal{L}[\hat{a} - i\hat{b}]$ (assuming the chiral limit for simplicity).

The result we find is that there are five slow rates. These mix the various populations and coherences of the cat state tensor products. The approximate scaling of all these rates with the drive strength goes as,

$$E_{\text{slow}} \sim \frac{J\lambda}{U} e^{-\frac{4\lambda}{U}} + \mathcal{O}\left(e^{-\frac{5\lambda}{U}}\right). \quad (4.34)$$

Note that we omit prefactors of order one. This result is in line with the single KPO from

Eq. (4.13), where that rate maps to one of the five here. The actual values and corresponding eigenvectors are detailed in Appendix C. The reason for the strong exponential scaling is the vanishing overlap between coherent states, $\langle +\alpha | -\alpha \rangle = e^{-2|\alpha|^2}$.

The conclusion to take away from this is that unlike the single KPO, we cannot choose a clever initial condition that will bypass the slow rates. Back then, the only slow rate was a population transfer between the two coherent eigenstates. We were able to choose a vacuum initial state that had equal overlap with both $|\alpha\rangle$ and $|- \alpha\rangle$, which allowed half the population to go to each one. In the two-cavity problem, the multiple rates mix up all populations and coherences of all four cat combinations in nontrivial ways. While cavity A will still obey the same master equation in the chiral limit, the necessary cavity-cavity correlations for the entangled cat will take a long time to reach, even if starting from vacuum.

In the following sections, we will evaluate the effects of unwanted losses for realistic experimental parameters. As it turns out, we can still get good fidelities with our desired entangled cats.

4.6.2 Intrinsic loss

Assuming a synthetic reservoir implementation in cQED, we take our cavities to have a leakage rate κ ,

$$\frac{d}{dt}\rho = -i[\hat{H}_{\text{EC}}, \rho] + 2\Gamma\mathcal{L}[\hat{a} - i\hat{b}] + \kappa\mathcal{L}[\hat{a}]\rho + \kappa\mathcal{L}[\hat{b}]\rho. \quad (4.35)$$

Kerr nonlinearities in cQED cavities can be made on the order of 100 KHz to 1 MHz [9]. State-of-the art 3D microwave cavities have leakage rates on the order of 100 Hz [92, 93]. This means that $\kappa/U = 10^{-3}$ to 10^{-4} are reasonable values to consider. We will use a conservative choice of $\kappa/U = 10^{-3}$ in the following simulations.

In Figure 4.8(a) we plot the numerically-computed fidelity of the system steady-state in terms of loss rate κ/U with the exact steady-state $|\psi_e\rangle$. The plot also shows fidelities with the ideal entangled cat from the the first line of Eq. (4.28), although we will focus on the

exact solution fidelity in this section.

We find that for our experimentally-viable limit of $\kappa/U = 10^{-3}$, we can still get good fidelities upwards of $F > 0.85$ with a value of $J/U = 1$, $\lambda/U = 2$. As suggested by our earlier discussion on the role of J , this choice of parameters still yields a good cat state. Taking higher J/U will cause the state to no longer be cat-like, even if it has high loss tolerance.

This result can be further improved by deviating away from nonreciprocity. Recall that we are free to tune the dissipator and coherent coupling separately. Fig. 4.8(b) plots the fidelity for $J/U = 1$, $\lambda/U = 2$ and $\kappa/U = 10^{-3}$ in terms of the nonchirality ratio Γ/J . We find that the fidelity with the exact state can be further improved to $F > 0.9$, corresponding to a cat fidelity of $F > 0.86$.

While these improvements are marginal, they also act as a good demonstration that we do not benefit from deviating *too* far from the chiral limit. We can do a little better, and have some wiggle room in the parameters, as long as we stay close.

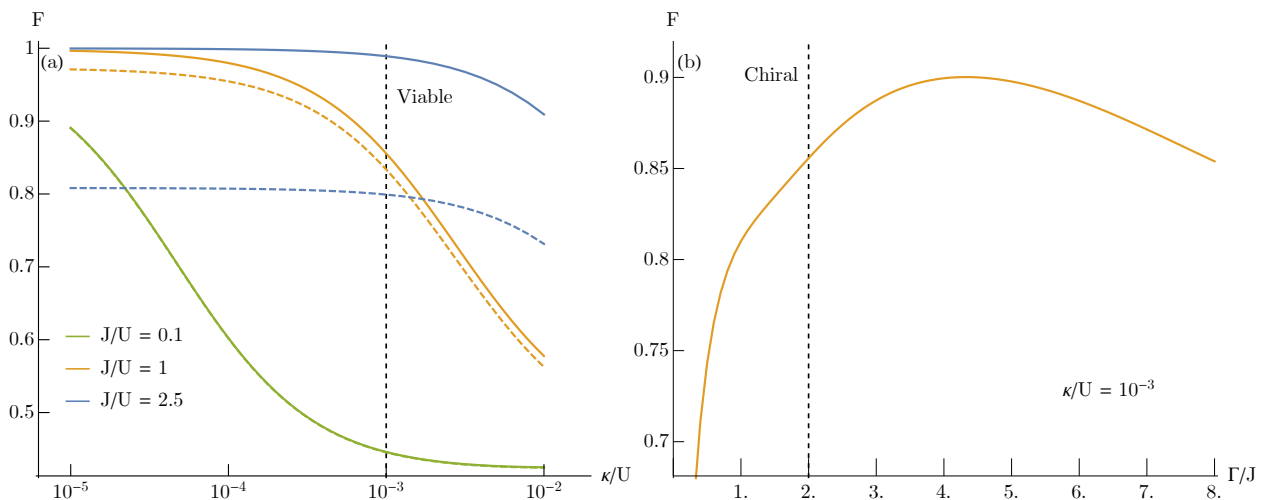


Figure 4.8: (a) Fidelity of the numerically computed steady-state for the two-cavity system, compared to the expected exact result $|\psi_e\rangle\langle\psi_e|$ (solid lines), and the ideal entangled cat state from the first line of Eq. (4.28) (dashed lines, accounting for an overall phase rotation). We plot in terms of decay rate κ/U . The drive strength is fixed at $\lambda/U = 2$. The dissipator strength is $\Gamma/U = 2$, which is the chiral limit (for simplicity). The black dashed line represents $\kappa/U = 10^{-3}$, which we claim to be the (conservatively-chosen) limit for experimental viability. (b) Fidelity in terms of nonchirality Γ/J , for $J/U = 1$, $\lambda/U = 2$ and loss $\kappa/U = 10^{-3}$.

4.6.3 Parameter mismatch

Aside from intrinsic loss, another concern is the mismatch of parameters. The perfect absorber recipe requires symmetric drive strengths and Kerr nonlinearities between the two cavities. To model such imperfections, we consider the following modified Hamiltonian,

$$\hat{H}_{\text{PM}} = \lambda(\hat{a}\hat{a} + h.c.) + \lambda(1 + \delta\lambda)(\hat{b}\hat{b} + h.c.) + U\hat{a}^\dagger\hat{a}^\dagger\hat{a}\hat{a} - U(1 + \delta U)\hat{b}^\dagger\hat{b}^\dagger\hat{b}\hat{b} + J(\hat{a}^\dagger\hat{b} + h.c.). \quad (4.36)$$

The dimensionless parameters $\delta\lambda$ and δU quantify how badly cavity B is mismatched to cavity A. We recover the perfect absorber for $\delta\lambda = \delta U = 0$.

In Fig. 4.9, we plot the fidelity of the setup in terms of $\delta\lambda$ and δU . The slow rates do not limit the system in this case, as we can attain fidelities above $F = 0.9$ even when the mismatch parameters greatly exceed E_{slow} . Since the mismatch does not damage the parity of the system, it is nowhere near as dangerous as transmission loss.

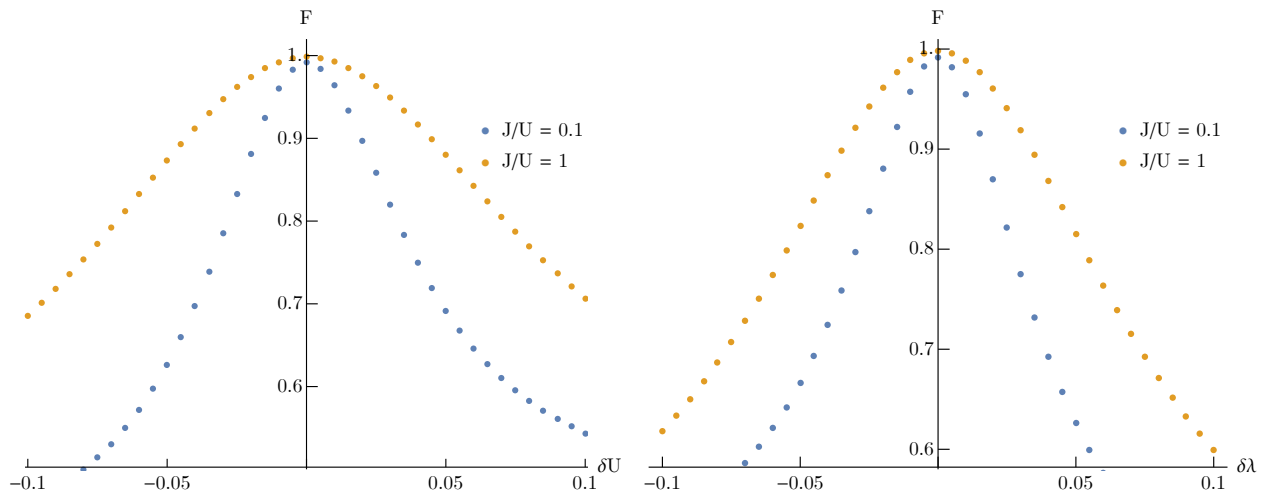


Figure 4.9: Fidelity of the numerically computed steady-state with $|\psi_e\rangle$ in terms of drive mismatch $\delta\lambda$ (left) and Kerr nonlinearity mismatch δU (right). The drive strength is fixed at $\lambda/U = 2$. The Hilbert space is truncated at $N = 12$ Fock states for each cavity.

4.7 Conclusion

This chapter gave a simple, explicit recipe for making entangled cat states. The exact setup with the necessary parameter restrictions is,

$$\begin{aligned}\hat{H}_{\text{EC}} &= \lambda(\hat{a}\hat{a} + \hat{b}\hat{b} + h.c.) + U(\hat{a}^\dagger\hat{a}^\dagger\hat{a}\hat{a} - \hat{b}^\dagger\hat{b}^\dagger\hat{b}\hat{b}) + J(\hat{a}^\dagger\hat{b} + h.c.), \\ \frac{d}{dt}\rho &= -i[\hat{H}_{\text{EC}}, \rho] + 2\Gamma\mathcal{L}[\hat{a} - i\hat{b}]\rho.\end{aligned}\tag{4.37}$$

The J -proportional term may also be replaced by a cavity detuning term $\delta(\hat{a}^\dagger\hat{a} - \hat{b}^\dagger\hat{b})$. The resulting pure steady-state will be $|\psi_e\rangle$ from Eq. (4.24).

Table 4.1: Experimentally-realistic values for the system parameters of the cat-generating scheme.

Parameter	Description	Regime
κ/U	Intrinsic loss rate.	Experimentally realistic values are $\kappa/U \sim 10^{-4} - 10^{-3}$.
λ/U	Parametric drive strength. Increasing it yields a more catlike state with higher α , but makes the system's loss tolerance and equilibration time longer.	For our chosen loss rates, the best drive strength to use is $\lambda/U \approx 2 - 2.5$.
J/U	Coherent coupling strength. Increasing it yields higher loss tolerance, but less catlike behaviour.	For our chosen drive strengths, the best value to use is $J/U \approx 1$.
Γ/U	Engineered dissipation strength. Deviating too far from the coherent coupling will weaken the loss tolerance.	For best loss tolerance, $\Gamma/U \approx J/U$.

Table 4.1 summarizes the relevant parameters of the system, and gives explicit prescriptions for realistic values that these parameters should take in an experiment.

This scheme only uses local interactions and nonlinearities, requiring no time-dependent elements. It is straightforward to realize, and has acceptable tolerance to experimentally-realistic losses.

Chapter 5

Adiabatic ramping

Throughout this thesis, we have mostly been concerned with the steady-state. The transient dynamics are more difficult to measure, and not as relevant to our stabilization schemes. Indeed, one of the biggest advantages of our system is that it creates *steady* entanglement.

However, the slow relaxation rates cause the system to take an extremely long time to reach the steady-state, compared to the natural scales in the problem. We already saw this in Fig. 4.4. For the Kerr setup, the problem is just as prominent because the slow rates scale in the same way.

To expedite the process of reaching the steady-state, we will add a slow time-dependence to our parametric drives. While the Kerr nonlinearities are not easy to modify mid-evolution, an experimental setup will have good control over the parametric drive strength. Recall from Eq. (4.34) that the slow rates also scale with the drive strength. For a small drive, the rates will only be proportional to the engineered dissipator strength Γ . For larger drives, they are exponentially suppressed by $e^{-4\lambda/U}$. Thus when $\lambda/U \ll 1$ the system will quickly equilibrate to the desired steady-state. We can remain in this desired steady-state by smoothly increasing the drive strength in an adiabatic ramp [94]. In effect, we ‘drag’ our system to the desired high-drive state in an adiabatic evolution.

The slope of this ramp must be larger than the slow rates, to prevent them from mixing the state, and smaller than the gap to the fast rates so that we do not access other eigenstates

of the Hamiltonian.

Note that this chapter will contain representative proof-of-concept results rather than optimized ramp shapes. The study of adiabatic ramping goes beyond the scope of this thesis. We seek only to show the benefit of introducing slow time dependence to our drives. As we will find in the last section of this short chapter, an adiabatic ramp will not only speed up the stabilization, but also allow us to reach *better* fidelities than the steady-state in the presence of loss.

5.1 Stabilization speedup

We will subject our drives to a simple ramp of the form,

$$\lambda(t) = \frac{\lambda}{1 + e^{-k(t-t_{\text{mid}})}}, \quad (5.1)$$

for a ramp time from $t = 0$ to $t = 2t_{\text{mid}}$. The slope of the ramp is set by k , with higher values corresponding to steeper (faster) ramps. The midpoint of the ramp t_{mid} is chosen such that $\lambda(t) \geq 0.99\lambda$ by the end of the ramp. We thus evolve from $\lambda(0) = 0.01\lambda$ to $\lambda(2t_{\text{mid}}) = 0.99\lambda$. Since the rates of the system are so fast for small drives, it is not a problem that we do not start exactly from zero drive amplitude.

In Fig. 5.1, we compare the fidelity of the system with the exact steady-state $|\psi_e\rangle$ and its undesired odd counterpart $|\psi_o\rangle$, for non-ramped and ramped dynamics. The unramped drives have $\lambda(t) = \lambda\Theta(t)$, with step function $\Theta(t)$ turning the drive on to maximum at the start of the evolution. The ramped drives obey Eq. (5.1). Since we do not consider loss, both the ramped and non-ramped systems will eventually reach $F = 1$. However, the unramped system takes an exponentially longer time in doing so. For parameters of $\lambda/U = 3$, $J/U = 1$, the ramped system reaches a fidelity of $F > 0.95$ in $tU \sim 10$. Note that we chose a higher drive strength than the previous chapter to emphasize the advantage that the ramp brings. In comparison, the non-ramped system will require $tU \sim 500$ to reach the same fidelity. We

see a significant speedup for the ramped case.

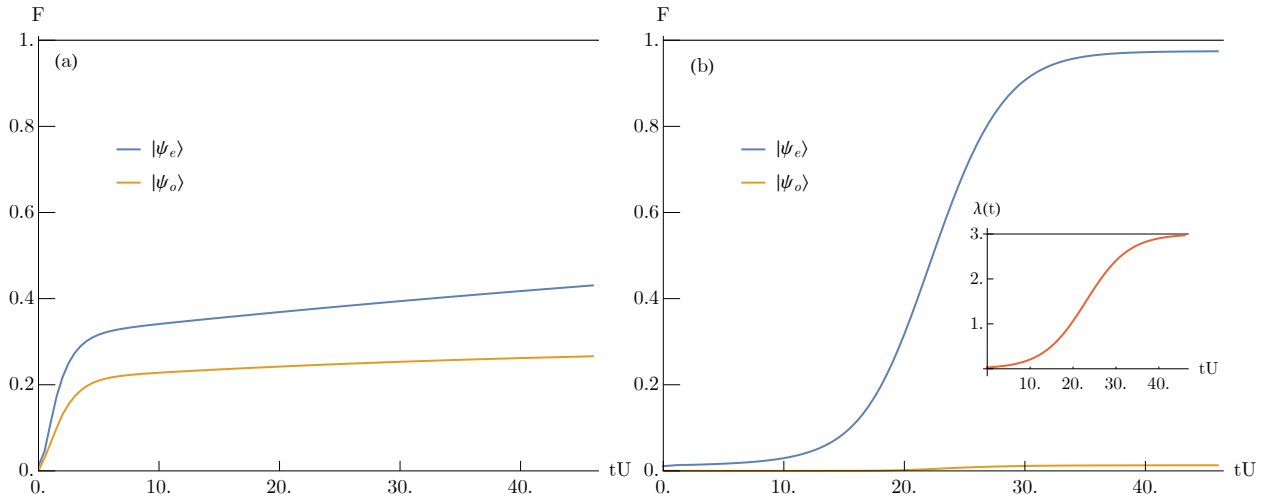


Figure 5.1: Fidelity of the time-dependent two-cavity system state with $|\psi_e\rangle$ and $|\psi_o\rangle$. We fix $J/U = 1$, measuring time t in units of $U = 1$. The system is initialized in the vacuum state. In panel (a), we initialize the drives at their maximum value of $\lambda/U = 3$, while in panel (b) we ramp them to this maximum value using the formula in Eq. (5.1) for $k/U = 0.2$, $t_{\text{mid}} = 23$. The ramp shape is plotted in the inset. The dissipator strength is set to $\Gamma/U = 0.5$, half the chiral limit, which we found to be the approximate best choice via numerics.

5.2 Metastable entangled-cat generation

If there is intrinsic loss in the system, the steady-state will no longer have 100% fidelity with the desired result $|\psi_e\rangle$. We have shown in the previous chapter that we still get good fidelities of $F > 0.9$ for reasonable experimental parameters and cat sizes. However, the adiabatic ramp can let us do better than the steady-state.

The ramp drags the system towards a desired state, bypassing the slow rates. While the fidelity will eventually decay back down to the steady-state result, we can still make use of the cat before this happens. The metastability provides a sufficient time window for the state to be transported away for use in another part of the system.

This concept is summarized in Fig. 5.2, which plots the time-dependent fidelity for a lossy system described by Eq. (4.35), with and without the time-dependent ramp of the drives. We choose parameters for which the steady-state has poor fidelity $F \approx 0.6$. If there

is no ramp, then the system takes a long time to reach the steady-state, but remains useless throughout the evolution.

On the other hand, if we have a ramp, then it lets the system quickly approach a high-fidelity state above the steady value. It then remains there for a long period of time, set by the intrinsic loss rate κ/U .

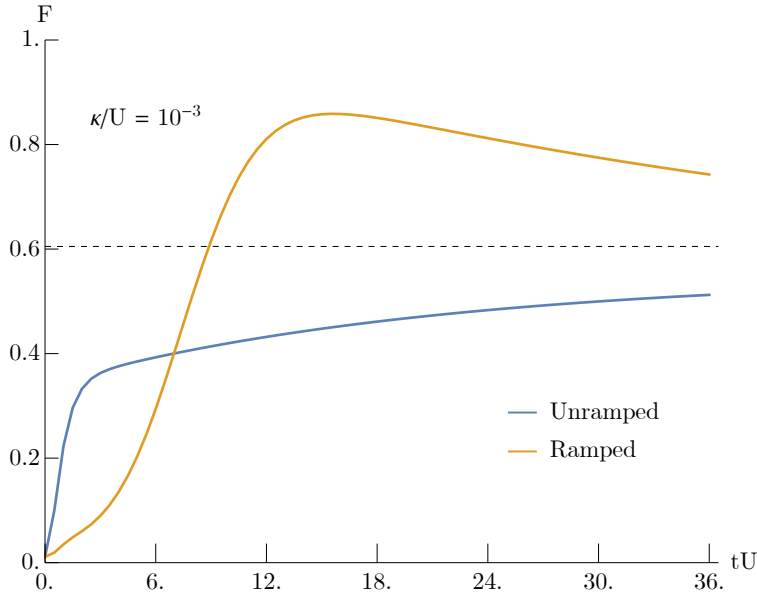


Figure 5.2: Fidelity of the time-dependent two-cavity system state with $|\psi_e\rangle$. We measure time t in units of $U = 1$. The system is initialized in the vacuum state. The ramp parameter is $k/U = 0.2$, corresponding to a ramp length of $2t_{\text{mid}} = 46$. The coherent coupling is $J/U = 1$ and the engineered dissipation is $\Gamma/U = 0.5$ (found to be the approximately optimal value for this set of parameters). The drive strength is set to $\lambda/U = 3$, and the decay rate at $\kappa/U = 10^{-3}$, for which the steady-state fidelity is $F \approx 0.6$ (indicated by the dashed line).

The choice of ramp parameter k plays an important role in just how high-fidelity we can get. Fig. 5.3 plots the peak fidelity that our ramped system will reach before it starts decaying back down. In the limit of $k/U \gg 1$, the ramp is identical to a quench where we initialize the drives at their maximum values, for which the slow rates inhibit us via metastability. For $k/U \ll 1$, the ramp takes so long that the slow rates ‘undo’ any adiabatic dynamics it creates on the go.

We see that for all drive strengths, assuming a coupling of $J/U = 1$, the optimal value is $k/U \approx 0.1 - 0.2$. The reason that this does not get scaled down by the exponentially-smaller

slow rates is because the ramp needs to be as steep as possible, without hitting the *fast* rates of the system. Since these fast rates do not exhibit the same exponential scaling in λ/U , we can go to higher drives and still get good metastable fidelities despite the steady-state being very bad.

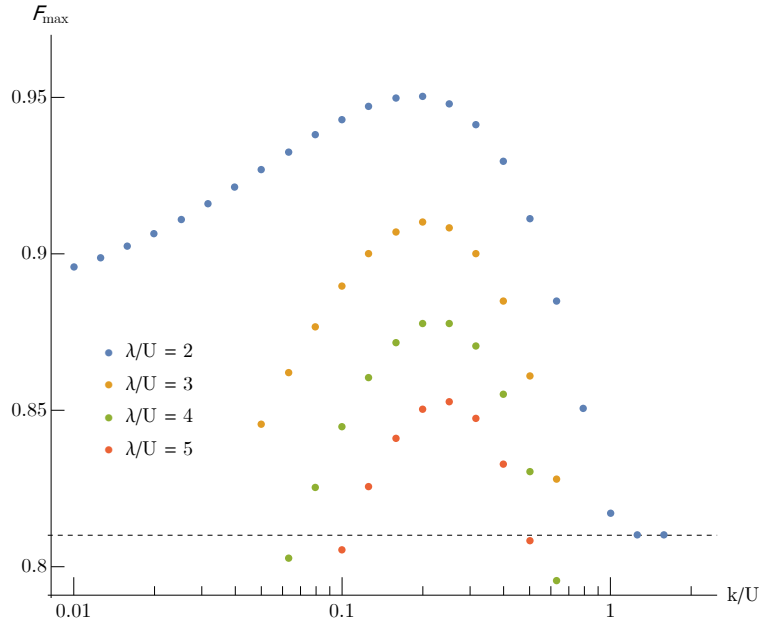


Figure 5.3: Peak fidelity of the ramped time-dependent two-cavity system state with $|\psi_e\rangle$ in terms of ramp parameter k/U . The system is initialized in the vacuum state. The coherent coupling is $J/U = 1$ and the engineered dissipation is $\Gamma/U = 0.5$. The decay rate is $\kappa/U = 10^{-3}$. For the λ/U line, the steady-state fidelity is shown with the dashed line. For very steep ramps indistinguishable from unramped systems, the system simply reaches the steady-state without going over.

Note that the choice of the nonchirality parameter Γ/J can also affect these results. Our empirical numeric observations have suggested $\Gamma/J \approx 0.5$ as the optimal value, which we have used in Fig. 5.3. It is challenging to produce analytic results in this regard, because we are now looking at transient dynamics for a time-dependent Hamiltonian with both dissipation and multiple slow rates.

The pursuits of finding more optimal ramps and getting a better analytical handle on the nonchirality ratio remain future goals for this work. Nonetheless, we have shown that with a simple, smooth adiabatic time-dependence for our system drives, we can generate entangled cats faster and with higher fidelity.

Chapter 6

Conclusion and outlook

The original goal of this thesis was to generate entangled states between bosonic cavities. We have given an explicit recipe for making two-mode squeezed states in Sec. 3.1, and entangled cat states in Sec. 4.2. What makes our setup stand out is the simplicity of the ingredients involved. The only nonlinearity we need is a self-Kerr interaction, which is well-known and easy to implement. All parametric drives in our system are local, which means that this two-cavity setup can easily be extended to an entire network. Moreover, we have shown that the system does not even need to have a coherent coupling between the cavities, instead replaced by cavity detunings. These advantages are crucial with the prospect of quantum computation and scaling in mind.

There are many extensions to pursue for this research in the future. The first and foremost is the prospect of tuning the cat-generating system to make it more resistant to loss. If true chiral waveguides using circulator-based implementations can have their loss rates improved by at least an order of magnitude, our scheme provides a way of easy remote entanglement for distant cavities. There are also ways of improving resilience through continuous parity measurements [22]. Since unwanted single-photon loss takes us from $|\psi_e\rangle$ to $|\psi_o\rangle$, flipping the parity, a circuit element that makes odd-parity states disfavoured will encourage the stabilization of just $|\psi_e\rangle$.

One can also consider far more sophisticated adiabatic ramps. Aside from driving the

system into the steady-state faster, ramps can bring us into a metastable state close to the unique one that we were after, allowing the system to remain stuck in it due to the slow rates. The ramp shape we provided is sufficient to show that good fidelities and short preparation times can be attained. Both these properties can be made higher through a rigorous mathematical choice of optimized ramp function.

Aside from easier ways to generate the state, there are also questions about what kind of state is actually needed for continuous-variable quantum computation. Our setup can generate cats with $\alpha \geq 1$, which are suitable according to the literature. However, our setup can also generate states that are very different from regular cats, but maintain high entanglement and strong nonlinearity (as evidenced by negative Wigner functions). If both the drive and coherent coupling greatly exceed the Kerr nonlinearity, we instead end up with a squeezed entangled cat. There is no inherent reason for why regular cats are the only viable state. The utility of such alternate states is also worth exploring further.

Lastly, the work in this thesis has helped shed more light on the perfect absorber recipe. This is a powerful tool for generating pure entangled states, but the requirements for it to work remain mysterious in present literature. We have given intuition in Appendix B on how the two gauge-invariant phases in the system act as effective magnetic fluxes in two rings, with one of them requiring maximally broken time-reversal symmetry. We have also shown that the recipe can work in the absence of broken time-reversal symmetry, despite being initially conceived as part of a cascaded quantum system. This gives fresh insight into the pursuit of entangled states for continuous-variable systems in the future.

Appendix A

Covariance matrix evolution

In this appendix, we will show how to find the covariance matrix for a quadratic two-mode system, following Appendix B in Ref. [95]. Assume that the system's equations of motion can be written as,

$$\begin{aligned}\hat{H} &= \hat{c}^T \hat{h} \hat{c}, \\ \frac{d}{dt} \rho &= -i[\hat{H}, \rho] + \sum_k \gamma_k \mathcal{L}[R_k^T \hat{c}] \rho.\end{aligned}\tag{A.1}$$

Here, $\hat{c} = \{\hat{x}_A, \hat{p}_A, \hat{x}_B, \hat{p}_B\}$ are the quadratures of the two cavity modes [(c.f. Eq. (3.18)]. The 4×4 matrix \hat{h} describes the Hamiltonian dynamics. The R_k are four-element vectors mapping to the jump operator for each decay channel, while the γ_k are the corresponding decay rates. They can be collected into an overall matrix that describes the dissipation's contribution,

$$\hat{Z} = \sum_k \gamma_k R_k^* R_k^T.\tag{A.2}$$

We now define two further matrices,

$$\begin{aligned}\hat{Q} &= 2\hat{\sigma} \left[\hat{h} + \text{Im}(\hat{Z}) \right], \\ \hat{N} &= 2\hat{\sigma} \left[\text{Re}(\hat{Z}) \right] \hat{\sigma}^T,\end{aligned}\tag{A.3}$$

where $\hat{\sigma}$ contains the commutation relations of the quadratures,

$$\hat{\sigma} = \begin{pmatrix} 0 & 1 & 0 & 0 \\ -1 & 0 & 0 & 0 \\ 0 & 0 & 0 & 1 \\ 0 & 0 & -1 & 0 \end{pmatrix}. \quad (\text{A.4})$$

With these, we write down the equations of motion for the covariance matrix,

$$\frac{d}{dt}C = \hat{Q}C + C\hat{Q}^T + \hat{N}. \quad (\text{A.5})$$

This is a simple linear system of equations that may be solved for both transient dynamics and the steady-state limit. For transient dynamics starting at $t = 0$ with initial condition $C(0) = C_0$, the solution is given by,

$$C(t) = e^{\hat{Q}t}C_0e^{\hat{Q}^Tt} + \int_0^t d\tau e^{\hat{Q}(t-\tau)}\hat{N}e^{\hat{Q}^T(t-\tau)}. \quad (\text{A.6})$$

The steady-state covariance matrix $C(\infty)$ can be found by either taking $t \rightarrow \infty$ in the transient solution above, or more easily, just setting the left hand side of Eq. (A.5) to zero and solving for the coefficients of C .

The dynamical matrix \hat{Q} describes the coherent evolution due to the Hamiltonian and measurements by the reservoirs. The steady-state solution will be unique, provided that the system is stable. Stability can be determined from looking at the eigenvalues of \hat{Q} : they must all have negative real part. Moreover, with a stable system the steady-state will be unique, as any information about the initial condition will be exponentially suppressed in time. We can also obtain information about the time it takes to reach the steady state, by considering the magnitudes of the smallest (i.e. slowest) eigenvalues of \hat{Q} .

Appendix B

Gauge-invariant phases

The perfect absorber system we consider has two gauge-invariant phases. This is not immediately obvious, as there are four independent terms in the Lindblad master equation. This appendix will demonstrate how two of the four can be gauged away, and explain what the remaining two represent in physical terms.

In general, the Hamiltonian and master equation can be written as,

$$\begin{aligned}\hat{H}_{\text{NP}} &= J(e^{i\phi_J}\hat{a}^\dagger\hat{b} + h.c.) + \lambda_A(e^{i\phi_A}\hat{a}\hat{a} + h.c.) + \lambda_B(e^{i\phi_B}\hat{b}\hat{b} + h.c.), \\ \frac{d}{dt}\rho &= -i[\hat{H}_{\text{NP}}, \rho] + 2\Gamma\mathcal{L}[\hat{a} + e^{i\phi_\Gamma}\hat{b}]\rho,\end{aligned}\tag{B.1}$$

where ϕ_J , ϕ_A , ϕ_B and ϕ_Γ are arbitrary constant phases for the time being. We first make the substitution,

$$\hat{a} = e^{i\phi_J}\hat{a}',\tag{B.2}$$

which results in:

$$\begin{aligned}\hat{H}_{\text{NP}} &= J(\hat{a}'^\dagger\hat{a} + h.c.) + \lambda_A(e^{i(\phi_A+2\phi_J)}\hat{a}'\hat{a}' + h.c.) + \lambda_B(e^{i\phi_B}\hat{b}\hat{b} + h.c.), \\ \frac{d}{dt}\rho &= -i[\hat{H}_{\text{NP}}, \rho] + 2\Gamma\mathcal{L}[\hat{a}' + e^{i(\phi_\Gamma-\phi_J)}\hat{b}]\rho.\end{aligned}\tag{B.3}$$

Then, the phase on the cavity A drive can be removed with a second substitution,

$$\hat{a}' = e^{-i(\phi_A+2\phi_J)/2}\hat{a}'', \quad \hat{b} = e^{-i(\phi_A+2\phi_J)/2}\hat{b}', \quad (\text{B.4})$$

which gives,

$$\begin{aligned} \hat{H}_{\text{NP}} &= J(\hat{a}''^\dagger\hat{b}' + h.c.) + \lambda_A(\hat{a}''\hat{a}'' + h.c.) + \lambda_B(e^{i(\phi_B-\phi_A-2\phi_J)}\hat{b}'\hat{b}' + h.c.), \\ \frac{d}{dt}\rho &= -i[\hat{H}_{\text{NP}}, \rho] + 2\Gamma\mathcal{L}[\hat{a}'' + e^{i(\phi_\Gamma-\phi_J)}\hat{b}']\rho. \end{aligned} \quad (\text{B.5})$$

At this point, we are down to just two phases. These can no longer be removed with simple gauge transformations. We define them by,

$$\begin{aligned} \phi &= \phi_B - \phi_A - 2\phi_J, \\ \theta &= \phi_\Gamma - \phi_J. \end{aligned} \quad (\text{B.6})$$

Relabelling $\hat{a}'' \rightarrow \hat{a}$ and $\hat{b}' \rightarrow \hat{b}$ for simplicity, the equations of motion now become

$$\begin{aligned} \hat{H}_{\text{NP}} &= J(\hat{a}^\dagger\hat{b} + h.c.) + \lambda_A(\hat{a}\hat{a} + h.c.) + \lambda_B(e^{i\phi}\hat{b}\hat{b} + h.c.), \\ \frac{d}{dt}\rho &= -i[H_{\text{NP}}, \rho] + \Gamma\mathcal{L}[\hat{a} + e^{i\theta}\hat{b}]\rho. \end{aligned} \quad (\text{B.7})$$

Fig. B.1 shows a schematic diagram of what these two gauge-invariant phases represent. The dissipation acts as a non-reciprocal hopping from both cavities to the reservoir. If we consider the synthetic implementation discussed in Subsec. 3.3, the system would have three hopping terms. Normally, we would then have two relative phases between these hopping terms alone. However, since we operate in the Markovian limit where the reservoir can be modelled with the Lindblad form, it is invariant under an overall phase ($\mathcal{L}[e^{i\theta}\hat{z}] = \mathcal{L}[\hat{z}]$). Thus θ encapsulates an effective magnetic flux piercing the coupling triangle between the two cavities and the dissipator.

On the other hand, the second phase ϕ corresponds to the drives. Bosonic parametric

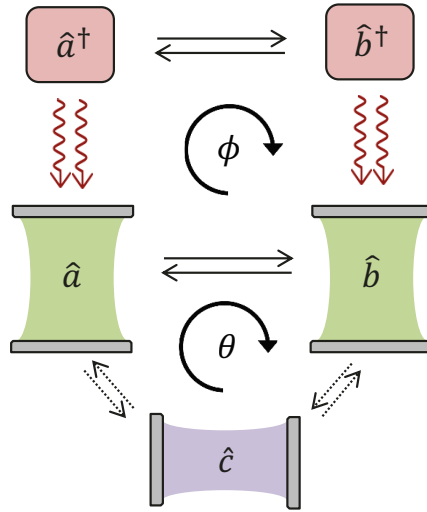


Figure B.1: Gauge-invariant phases of the two-cavity parametrically driven system from Eq. (B.7). The solid black lines are J -proportional coherent coupling terms. The λ_A, λ_B -proportional parametric drives are in red, corresponding to effective tunneling between particle and hole modes. The dotted black lines are Γ -proportional dissipative couplings to an auxiliary cavity acting as a reservoir. The two phases are encircled by two coupling loops, with θ corresponding to the dissipative couplings, and ϕ the particle-hole parametric drive couplings.

driving Hamiltonians have an inherent particle-hole symmetry [1], meaning that we can treat \hat{a}^\dagger as an annihilation operator for a new mode populated by holes rather than particles. A drive term of the form $(\hat{a}\hat{a} + h.c.)$ can then be thought of as hopping between this hole mode and the corresponding particle mode (c.f. Fig. B.1). Since the tunneling term $(\hat{a}^\dagger\hat{b} + h.c.)$ cannot distinguish between particles and holes, the hole modes are also coupled by it. All in all, the parametric drives enable a *second* effective magnetic flux piercing the cavity modes and their hole counterparts.

It is these two gauge-invariant phases that are used in the perfect absorber recipe. The lower one θ must be fixed at $\theta = \pm\pi/2$ to maximally break time-reversal symmetry and enable non-reciprocity. On the other hand, the upper one ϕ must be zero, since any other value would create a sort of reverse process, helping to re-establish the symmetry we wanted to break. Note that self-Kerr nonlinearities do not break any of these arguments, because they are invariant under the gauge transformations we make.

If we instead consider the detuning-based implementation from Sec. 4.5, the central J -

dependent couplings are absent. There are thus no central fluxes enclosed in any loops, and thus no time-reversal symmetry breaking. We can choose a gauge where all the system coefficients are real.

Appendix C

Two-cavity superoperator perturbation theory

This appendix will now repeat our superoperator-based degenerate perturbation theory for the two-cavity system. There are four relevant cat state tensor products,

$$\begin{aligned} |\phi_1\rangle &= |\mathcal{C}_+(i\alpha)\rangle \otimes |\mathcal{C}_+(\alpha)\rangle, \\ |\phi_2\rangle &= |\mathcal{C}_+(i\alpha)\rangle \otimes |\mathcal{C}_-(\alpha)\rangle, \\ |\phi_3\rangle &= |\mathcal{C}_-(i\alpha)\rangle \otimes |\mathcal{C}_+(\alpha)\rangle, \\ |\phi_4\rangle &= |\mathcal{C}_-(i\alpha)\rangle \otimes |\mathcal{C}_-(\alpha)\rangle. \end{aligned} \tag{C.1}$$

The amplitude $\alpha = \sqrt{\lambda/U}$ is the same as in the single-oscillator case. These states are orthonormal degenerate eigenstates of the two onsite Hamiltonians in combination:

$$(\hat{H}_A + \hat{H}_B) |\phi_i\rangle = 0. \tag{C.2}$$

The problem can now be cast as,

$$\begin{aligned}
\frac{d}{dt}\rho &= L_0\rho + L_1\rho, \\
L_0\rho &= -i[\hat{H}_A + \hat{H}_B, \rho], \\
L_1\rho &= -iJ[\hat{a}^\dagger\hat{b} + h.c., \rho] + 2J\mathcal{L}[\hat{a} - i\hat{b}]\rho.
\end{aligned} \tag{C.3}$$

The unperturbed part L_0 is two independent Kerr parametric oscillator systems, for which $|\phi_j\rangle$ are zero-energy eigenstates. Meanwhile, L_1 connects them with a J -proportional non-reciprocal tunneling interaction. The superoperators can be rewritten as matrices via,

$$\begin{aligned}
L_0 &= -i \left[\mathbb{1} \otimes (\hat{H}_A + \hat{H}_B) - (\hat{H}_A + \hat{H}_B)^* \otimes \mathbb{1} \right], \\
L_1 &= -i \left(\mathbb{1} \otimes \hat{H}_J - \hat{H}_J^* \otimes \mathbb{1} \right) + 2J \left[(\hat{a} + i\hat{b}) \otimes (\hat{a} - i\hat{b}) - \frac{1}{2} \mathbb{1} \otimes (\hat{a}^\dagger + i\hat{b}^\dagger)(\hat{a} - i\hat{b}) \right. \\
&\quad \left. - \frac{1}{2}(\hat{a}^\dagger - i\hat{b}^\dagger)(\hat{a} + i\hat{b}) \otimes \mathbb{1} \right].
\end{aligned} \tag{C.4}$$

There are sixteen basis states for the superoperators to act on, consisting of all possible outer products $|\phi_i\rangle\langle\phi_j|$. Following the degenerate perturbation theory calculation, we express L_1 in this basis and diagonalize it. For the sanity of the reader, we will omit the explicit 16×16 resulting matrix here, noting only that it is proportional to $J\alpha^2$ and non-Hermitian as expected.

Before going to the results, we are also going to make another basis change to help our intuitive understanding. We define the following four states,

$$\begin{aligned}
|\psi_1\rangle &= \frac{1}{\sqrt{2}} (|\phi_1\rangle + |\phi_4\rangle), \\
|\psi_2\rangle &= \frac{1}{\sqrt{2}} (|\phi_2\rangle + |\phi_3\rangle), \\
|\psi_3\rangle &= \frac{1}{\sqrt{2}} (|\phi_1\rangle - |\phi_4\rangle), \\
|\psi_4\rangle &= \frac{1}{\sqrt{2}} (|\phi_2\rangle - |\phi_3\rangle).
\end{aligned} \tag{C.5}$$

The first two states map back to the even and odd-parity solutions to the Kerr system's

recursion relations, i.e. $|\psi_1\rangle = |\psi_e\rangle + \mathcal{O}(e^{-2\alpha^2})$, and $|\psi_2\rangle = |\psi_o\rangle + \mathcal{O}(e^{-2\alpha^2})$. These are the exact and approximate steady-states we expect in the model. The other two states $|\psi_3\rangle$, $|\psi_4\rangle$ are an analogous pair for the system with opposite chirality, $\mathcal{L}[\hat{a} + i\hat{b}]$. We keep all four states in the calculation because they act as four effective Bell states for a qubit, and span the subspace of interest.

Going back to the perturbation theory, we find sixteen eigenvalues and eigenvectors. Only six of these have an eigenvalue that becomes small in the limit of strong driving. In what follows, we will write the eigenvalue E_i to lowest nonzero order in $e^{-\alpha^2}$, and the eigenvector $|E_i\rangle\rangle$ to zeroth order in the same quantity, just to keep things simple.

The first slow eigenvector is the unique steady-state:

$$\begin{aligned} E_1 &= 0, \\ |E_1\rangle\rangle &\approx (|\psi_1\rangle\langle\psi_1|)_v. \end{aligned} \tag{C.6}$$

The next two degenerate eigenvectors represent decay in the coherences between $|\psi_1\rangle$ and $|\psi_2\rangle$:

$$\begin{aligned} E_2 = E_3 &\approx -4J\alpha^2 e^{-4\alpha^2}, \\ |E_2\rangle\rangle &\approx (|\psi_1\rangle\langle\psi_2|)_v, \\ |E_3\rangle\rangle &\approx (|\psi_2\rangle\langle\psi_1|)_v, \end{aligned} \tag{C.7}$$

The next two eigenvectors represent combined decay in the state populations:

$$\begin{aligned} E_4 &\approx -2J\alpha^2(7 + \sqrt{17})e^{-4\alpha^2}, \\ |E_4\rangle\rangle &\approx \left[(9 + \sqrt{17})|\psi_1\rangle\langle\psi_1| + (1 + \sqrt{17})|\psi_2\rangle\langle\psi_2| - (5 + \sqrt{17})(|\psi_3\rangle\langle\psi_3| + |\psi_4\rangle\langle\psi_4|) \right]_v, \\ E_5 &\approx -2J\alpha^2(7 - \sqrt{17})e^{-4\alpha^2}, \\ |E_5\rangle\rangle &\approx \left[(9 - \sqrt{17})|\psi_1\rangle\langle\psi_1| + (1 - \sqrt{17})|\psi_2\rangle\langle\psi_2| - (5 - \sqrt{17})(|\psi_3\rangle\langle\psi_3| + |\psi_4\rangle\langle\psi_4|) \right]_v. \end{aligned} \tag{C.8}$$

Finally, there is an eigenvector corresponding to combined decay in the state coherences:

$$E_6 \approx -20J\alpha^2 e^{-4\alpha^2}, \quad (\text{C.9})$$

$$|E_6\rangle \approx (|\psi_1\rangle\langle\psi_2| + |\psi_2\rangle\langle\psi_1| + |\psi_3\rangle\langle\psi_4| + |\psi_4\rangle\langle\psi_3|)_v.$$

All of these eigenvalues scale with α in the same way. This scaling is the same as in the one cavity problem [c.f. Eq. (4.13)], up to prefactors of order one. We can thus expect that in the regime where our perturbation theory is valid, all of these processes will be active for roughly the same time scale (up to one order of magnitude).

Fig. C.1 plots the effective spectrum of the full Liouvillian for the two cavity system. We obtain the five smallest-real part nonzero eigenvalues of $L_0 + L_1$, and plot them in terms of the drive strength. The expected scaling holds as long as we have $\alpha^2 = \lambda/U \geq 1$. Note that the plot will experience deviations as we continue increasing the drive strength, similar to what we saw in Fig. 4.3. Accounting for those will require higher-order perturbation theory. However, since these deviations will cause us to underestimate the slow rate, we can still use the analytic scaling as a worst-case scenario.

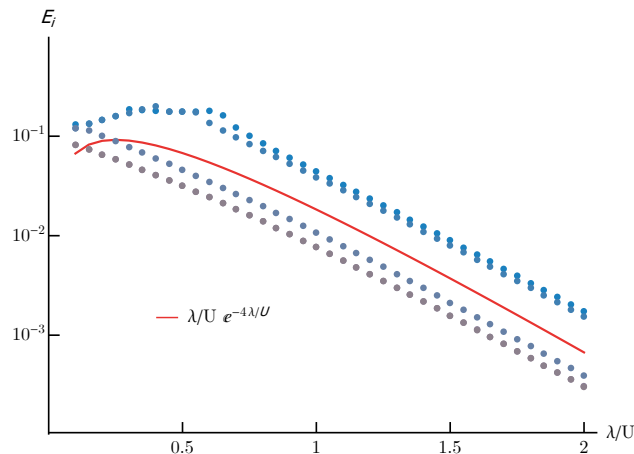


Figure C.1: Slow rates of the two-cavity system in Eq. (C.3), obtained from the five smallest-real part nonzero eigenvalues of $L_0 + L_1$. We plot in terms of the drive strength $\lambda/U = \alpha^2$, and fix $J/U = 0.1$. We assume the chiral limit $J = \Gamma$. The solid red line is the expected scaling with the drive strength, $\alpha^2 e^{-4\alpha^2}$, with no prefactors. The Hilbert space is truncated to $N = 12$ Fock states per cavity.

The conclusion is that the process of reaching the steady-state will be inhibited by a rate

on the order of $\alpha^2 e^{-4\alpha^2}$. There are several different processes that will shuffle populations and coherences back and forth between the four relevant states $|\psi_i\rangle$, eventually stabilizing the unique steady-state $|\psi_1\rangle$.

Bibliography

- [1] SL Braunstein and P Van Loock. Quantum information with continuous variables. *Reviews of Modern Physics*, 77(2):513, 2005.
- [2] P van Loock. Quantum communication with continuous variables. *Fortschritte der Physik*, 50(12):1177–1372, 2002.
- [3] A Shacham, K Bergman, and LP Carloni. Photonic networks-on-chip for future generations of chip multiprocessors. *IEEE Transactions on Computers*, 57(9):1246–1260, 2008.
- [4] A Blais, RS Huang, A Wallraff, SM Girvin, and RJ Schoelkopf. Cavity quantum electrodynamics for superconducting electrical circuits: An architecture for quantum computation. *Physical Review A*, 69(6):062320, 2004.
- [5] MH Devoret, SM Girvin, and RJ Schoelkopf. Circuit-qed: How strong can the coupling between a josephson junction atom and a transmission line resonator be? *Annalen der Physik*, 16(10-11):767–779, 2007.
- [6] F Beaudoin, JM Gambetta, and A Blais. Dissipation and ultrastrong coupling in circuit qed. *Physical Review A*, 84(4):043832, 2011.
- [7] J Suh, MD LaHaye, PM Echternach, KC Schwab, and ML Roukes. Parametric amplification and back-action noise squeezing by a qubit-coupled nanoresonator. *Nano letters*, 10(10):3990–3994, 2010.

- [8] K Moon and SM Girvin. Theory of microwave parametric down-conversion and squeezing using circuit qed. *Physical Review Letters*, 95(14):140504, 2005.
- [9] G Kirchmair, B Vlastakis, Z Leghtas, SE Nigg, H Paik, E Ginossar, M Mirrahimi, L Frunzio, SM Girvin, and RJ Schoelkopf. Observation of quantum state collapse and revival due to the single-photon kerr effect. *arXiv preprint arXiv:1211.2228*, 2012.
- [10] FR Ong, M Boissonneault, F Mallet, A Palacios-Laloy, A Dewes, AC Doherty, A Blais, P Bertet, D Vion, and D Esteve. Circuit qed with a nonlinear resonator: ac-stark shift and dephasing. *Physical Review Letters*, 106(16):167002, 2011.
- [11] S Rebić, J Twamley, and GJ Milburn. Giant kerr nonlinearities in circuit quantum electrodynamics. *Physical Review Letters*, 103(15):150503, 2009.
- [12] DP DiVincenzo et al. The physical implementation of quantum computation. *arXiv preprint quant-ph/0002077*, 2000.
- [13] YD Wang, S Chesi, and AA Clerk. Bipartite and tripartite output entanglement in three-mode optomechanical systems. *Physical Review A*, 91(1):013807, 2015.
- [14] A Ourjoumtsev, F Ferreyrol, R Tualle-Brouri, and P Grangier. Preparation of non-local superpositions of quasi-classical light states. *Nature Physics*, 5(3):189–192, 2009.
- [15] C Joshi, J Larson, M Jonson, E Andersson, and P Öhberg. Entanglement of distant optomechanical systems. *Physical Review A*, 85(3):033805, 2012.
- [16] JF Poyatos, JI Cirac, and P Zoller. Quantum reservoir engineering with laser cooled trapped ions. *Physical Review Letters*, 77(23):4728, 1996.
- [17] P Rabl, A Shnirman, and P Zoller. Generation of squeezed states of nanomechanical resonators by reservoir engineering. *Physical Review B*, 70(20):205304, 2004.

- [18] A Sarlette, JM Raimond, M Brune, and P Rouchon. Stabilization of nonclassical states of the radiation field in a cavity by reservoir engineering. *Physical Review Letters*, 107(1):010402, 2011.
- [19] YD Wang and AA Clerk. Reservoir-engineered entanglement in optomechanical systems. *Physical Review Letters*, 110(25):253601, 2013.
- [20] MJ Woolley and AA Clerk. Two-mode squeezed states in cavity optomechanics via engineering of a single reservoir. *Physical Review A*, 89(6):063805, 2014.
- [21] CA Muschik, H Krauter, K Jensen, JM Petersen, JI Cirac, and ES Polzik. Robust entanglement generation by reservoir engineering. *Journal of Physics B: Atomic, Molecular and Optical Physics*, 45(12):124021, 2012.
- [22] M Mirrahimi, Z Leghtas, VV Albert, S Touzard, RJ Schoelkopf, L Jiang, and MH Devoret. Dynamically protected cat-qubits: a new paradigm for universal quantum computation. *New Journal of Physics*, 16(4):045014, 2014.
- [23] C Wang, YY Gao, P Reinhold, RW Heeres, N Ofek, K Chou, C Axline, M Reagor, J Blumoff, KM Sliwa, et al. A schrödinger cat living in two boxes. *Science*, 352(6289):1087–1091, 2016.
- [24] F Minganti, N Bartolo, J Lolli, W Casteels, and C Ciuti. Exact results for schrödinger cats in driven-dissipative systems and their feedback control. *Scientific reports*, 6, 2016.
- [25] B Vlastakis, G Kirchmair, Z Leghtas, SE Nigg, L Frunzio, SM Girvin, M Mirrahimi, MH Devoret, and RJ Schoelkopf. Deterministically encoding quantum information using 100-photon schrödinger cat states. *Science*, 342(6158):607–610, 2013.
- [26] WJ Munro, G Milburn, and BC Sanders. Entangled coherent-state qubits in an ion trap. *Physical Review A*, 62(5):052108, 2000.

- [27] A Gilchrist, K Nemoto, WJ Munro, TC Ralph, S Glancy, SL Braunstein, and GJ Milburn. Schrödinger cats and their power for quantum information processing. *Journal of Optics B: Quantum and Semiclassical Optics*, 6(8):S828, 2004.
- [28] TC Ralph, A Gilchrist, GJ Milburn, William J Munro, and S Glancy. Quantum computation with optical coherent states. *Physical Review A*, 68(4):042319, 2003.
- [29] AA Clerk, MH Devoret, SM Girvin, F Marquardt, and RJ Schoelkopf. Introduction to quantum noise, measurement, and amplification. *Reviews of Modern Physics*, 82(2):1155, 2010.
- [30] C Gerry and P Knight. *Introductory quantum optics*. Cambridge university press, 2005.
- [31] LA Wu, HJ Kimble, JL Hall, and H Wu. Generation of squeezed states by parametric down conversion. *Physical Review Letters*, 57(20):2520, 1986.
- [32] A Ourjoumtsev, H Jeong, R Tualle-Brouri, and P Grangier. Generation of optical ‘schrödinger cats’ from photon number states. *Nature*, 448(7155):784, 2007.
- [33] A Ourjoumtsev, R Tualle-Brouri, J Laurat, and P Grangier. Generating optical schrödinger kittens for quantum information processing. *Science*, 312(5770):83–86, 2006.
- [34] M Brune, S Haroche, JM Raimond, L Davidovich, and N Zagury. Manipulation of photons in a cavity by dispersive atom-field coupling: Quantum-nondemolition measurements and generation of “schrödinger cat” states. *Physical Review A*, 45(7):5193, 1992.
- [35] B Yurke and D Stoler. Generating quantum mechanical superpositions of macroscopically distinguishable states via amplitude dispersion. *Physical Review Letters*, 57(1):13, 1986.
- [36] KE Cahill and RJ Glauber. Density operators and quasiprobability distributions. *Physical Review*, 177(5):1882, 1969.

- [37] K Vogel and H Risken. Determination of quasiprobability distributions in terms of probability distributions for the rotated quadrature phase. *Physical Review A*, 40(5):2847, 1989.
- [38] G Lindblad. On the generators of quantum dynamical semigroups. *Communications in Mathematical Physics*, 48(2):119–130, 1976.
- [39] MB Plenio and PL Knight. The quantum-jump approach to dissipative dynamics in quantum optics. *Reviews of Modern Physics*, 70(1):101, 1998.
- [40] T Brandes. Chapter 7 (quantum dissipation), lectures on background to quantum information, 2004.
- [41] AA Budini. Lindblad rate equations. *Physical Review A*, 74(5):053815, 2006.
- [42] CA Brasil, FF Fanchini, and RJ Napolitano. A simple derivation of the lindblad equation. *Revista Brasileira de Ensino de Física*, 35(1):01–09, 2013.
- [43] VV Albert and L Jiang. Symmetries and conserved quantities in lindblad master equations. *Physical Review A*, 89(2):022118, 2014.
- [44] WE Arnoldi. The principle of minimized iterations in the solution of the matrix eigenvalue problem. *Quarterly of applied mathematics*, 9(1):17–29, 1951.
- [45] F Motzoi, E Halperin, X Wang, KB Whaley, and S Schirmer. Backaction-driven, robust, steady-state long-distance qubit entanglement over lossy channels. *Physical Review A*, 94(3):032313, 2016.
- [46] C Gonzalez-Ballester, A Gonzalez-Tudela, FJ Garcia-Vidal, and E Moreno. Chiral route to spontaneous entanglement generation. *Physical Review B*, 92(15):155304, 2015.
- [47] F Quijandría, D Porras, JJ García-Ripoll, and D Zueco. Circuit qed bright source for chiral entangled light based on dissipation. *Physical Review Letters*, 111(7):073602, 2013.

- [48] P Lodahl, S Mahmoodian, S Stobbe, P Schneeweiss, J Volz, A Rauschenbeutel, H Pichler, and P Zoller. Chiral quantum optics. *arXiv preprint arXiv:1608.00446*, 2016.
- [49] D Jalas, A Petrov, M Eich, W Freude, S Fan, Z Yu, R Baets, A Popovic, Mand Melloni, JD Joannopoulos, et al. What is—and what is not—an optical isolator. *Nature Photonics*, 7(8):579, 2013.
- [50] EJ Lenferink, G Wei, and NP Stern. Coherent optical non-reciprocity in axisymmetric resonators. *Optics express*, 22(13):16099–16111, 2014.
- [51] K Xia, G Lu, G Lin, Y Cheng, Y Niu, S Gong, J Twamley, et al. Reversible nonmagnetic single-photon isolation using unbalanced quantum coupling. *Physical Review A*, 90(4):043802, 2014.
- [52] C Sayrin, C Junge, R Mitsch, B Albrecht, D O’Shea, P Schneeweiss, J Volz, and A Rauschenbeutel. Nanophotonic optical isolator controlled by the internal state of cold atoms. *Physical Review X*, 5(4):041036, 2015.
- [53] DE Chang, V Vuletic, and MD Lukin. Quantum nonlinear optics—photon by photon. *Nature Photonics*, 8(9):685, 2014.
- [54] A Javadi, I Söllner, M Arcari, SL Hansen, L Midolo, S Mahmoodian, G Kiršanskė, T Pregonolato, EH Lee, JD Song, et al. Single-photon nonlinear optics with a quantum dot in a waveguide. *arXiv preprint arXiv:1504.06895*, 2015.
- [55] G Della Valle and S Longhi. Spectral and transport properties of time-periodic pt-symmetric tight-binding lattices. *Physical Review A*, 87(2):022119, 2013.
- [56] CW Gardiner. Driving a quantum system with the output field from another driven quantum system. *Physical Review Letters*, 70(15):2269, 1993.
- [57] HJ Carmichael. Quantum trajectory theory for cascaded open systems. *Physical Review Letters*, 70(15):2273, 1993.

- [58] A Metelmann and AA Clerk. Nonreciprocal photon transmission and amplification via reservoir engineering. *Physical Review X*, 5(2):021025, 2015.
- [59] N Sugimoto, T Shintaku, A Tate, H Terui, M Shimokozono, E Kubota, M Ishii, and Y Inoue. Waveguide polarization-independent optical circulator. *IEEE Photonics Technology Letters*, 11(3):355–357, 1999.
- [60] Wo Śmigaj, J Romero-Vivas, B Gralak, L Magdenko, B Dagens, and M Vanwolleghem. Magneto-optical circulator designed for operation in a uniform external magnetic field. *Optics letters*, 35(4):568–570, 2010.
- [61] J Combes, J Kerckhoff, and M Sarovar. The slh framework for modeling quantum input-output networks. *arXiv preprint arXiv:1611.00375*, 2016.
- [62] S Hagelin. Analysis of lossy symmetrical three-port networks with circulator properties. *IEEE Transactions on Microwave Theory and Techniques*, 17(6):328–333, 1969.
- [63] C Gardiner and P Zoller. *Quantum noise: a handbook of Markovian and non-Markovian quantum stochastic methods with applications to quantum optics*, volume 56. Springer Science & Business Media, 2004.
- [64] PD Drummond and DF Walls. Quantum theory of optical bistability. i. nonlinear polarisability model. *Journal of Physics A: Mathematical and General*, 13(2):725, 1980.
- [65] K Fang, J Luo, A Metelmann, MH Matheny, F Marquardt, AA Clerk, and O Painter. Generalized non-reciprocity in an optomechanical circuit via synthetic magnetism and reservoir engineering. *Nature Physics*, 2017.
- [66] K Stannigel, P Rabl, and P Zoller. Driven-dissipative preparation of entangled states in cascaded quantum-optical networks. *New Journal of Physics*, 14(6):063014, 2012.
- [67] A Furusawa, JeL Sørensen, SL Braunstein, CA Fuchs, HJ Kimble, and ES Polzik. Unconditional quantum teleportation. *Science*, 282(5389):706–709, 1998.

- [68] TC Ralph and PK Lam. Teleportation with bright squeezed light. *Physical Review Letters*, 81(25):5668, 1998.
- [69] PT Cochrane, TC Ralph, and GJ Milburn. Teleportation improvement by conditional measurements on the two-mode squeezed vacuum. *Physical Review A*, 65(6):062306, 2002.
- [70] M Ban. Quantum dense coding via a two-mode squeezed-vacuum state. *Journal of Optics B: Quantum and Semiclassical Optics*, 1(6):L9, 1999.
- [71] PM Anisimov, GM Raterman, A Chiruvelli, WN Plick, D Huver, H Lee, and JP Dowling. Quantum metrology with two-mode squeezed vacuum: parity detection beats the heisenberg limit. *Physical Review Letters*, 104(10):103602, 2010.
- [72] SL Braunstein and P Van Loock. Quantum information with continuous variables. *Reviews of Modern Physics*, 77(2):513, 2005.
- [73] G Adesso and F Illuminati. Entanglement in continuous-variable systems: recent advances and current perspectives. *Journal of Physics A: Mathematical and Theoretical*, 40(28):7821, 2007.
- [74] A Peres. Separability criterion for density matrices. *Physical Review Letters*, 77(8):1413, 1996.
- [75] K Koga and N Yamamoto. Dissipation-induced pure gaussian state. *Physical Review A*, 85(2):022103, 2012.
- [76] Z Cai and T Barthel. Algebraic versus exponential decoherence in dissipative many-particle systems. *Physical Review Letters*, 111(15):150403, 2013.
- [77] SJ Van Enk and O Hirota. Entangled coherent states: Teleportation and decoherence. *Physical Review A*, 64(2):022313, 2001.

- [78] X Wang. Quantum teleportation of entangled coherent states. *Physical Review A*, 64(2):022302, 2001.
- [79] TJ Johnson, SD Bartlett, and BC Sanders. Continuous-variable quantum teleportation of entanglement. *Physical Review A*, 66(4):042326, 2002.
- [80] H Jeong, MS Kim, and J Lee. Quantum-information processing for a coherent superposition state via a mixed entangled coherent channel. *Physical Review A*, 64(5):052308, 2001.
- [81] Ni Sangouard, C Simon, N Gisin, J Laurat, R Tualle-Brouri, and P Grangier. Quantum repeaters with entangled coherent states. *JOSA B*, 27(6):A137–A145, 2010.
- [82] NA Ansari, L Di Fiore, MA Man’ko, VI Man’ko, S Solimeno, and F Zaccaria. Quantum limits in interferometric gravitational-wave antennas in the presence of even and odd coherent states. *Physical Review A*, 49(3):2151, 1994.
- [83] Barry C Sanders. Review of entangled coherent states. *Journal of Physics A: Mathematical and Theoretical*, 45(24):244002, 2012.
- [84] WB Gao, CY Lu, XC Yao, P Xu, O Gühne, A Goebel, YA Chen, CZ Peng, ZB Chen, and JW Pan. Experimental demonstration of a hyper-entangled ten-qubit schrödinger cat state. *arXiv preprint arXiv:0809.4277*, 2008.
- [85] CC Gerry. Generation of schrödinger cats and entangled coherent states in the motion of a trapped ion by a dispersive interaction. *Physical Review A*, 55(3):2478, 1997.
- [86] C Arenz, C Cormick, D Vitali, and G Morigi. Generation of two-mode entangled states by quantum reservoir engineering. *Journal of Physics B: Atomic, Molecular and Optical Physics*, 46(22):224001, 2013.
- [87] P Weinberger. John kerr and his effects found in 1877 and 1878. *Philosophical Magazine Letters*, 88(12):897–907, 2008.

- [88] S Puri and A Blais. Engineering the quantum states of light in a kerr-nonlinear resonator by two-photon driving. *arXiv preprint arXiv:1605.09408*, 2016.
- [89] ACY Li, F Petruccione, and J Koch. Perturbative approach to markovian open quantum systems. *Scientific reports*, 4:4887, 2014.
- [90] VV Albert, B Bradlyn, M Fraas, and L Jiang. Geometry and response of lindbladians. *Physical Review X*, 6(4):041031, 2016.
- [91] SJ Van Enk and O Hirota. Entangled coherent states: Teleportation and decoherence. *Physical Review A*, 64(2):022313, 2001.
- [92] M Reagor, H Paik, G Catelani, L Sun, C Axline, E Holland, IM Pop, NA Masluk, T Brecht, L Frunzio, et al. Reaching 10 ms single photon lifetimes for superconducting aluminum cavities. *Applied Physics Letters*, 102(19):192604, 2013.
- [93] M Reagor, W Pfaff, C Axline, RW Heeres, N Ofek, K Sliwa, E Holland, C Wang, J Blumoff, K Chou, et al. A quantum memory with near-millisecond coherence in circuit qed, 2015. *arXiv preprint arXiv:1508.05882*, 2015.
- [94] C Marr, A Beige, and G Rempe. Entangled-state preparation via dissipation-assisted adiabatic passages. *Physical Review A*, 68(3):033817, 2003.
- [95] M Wallquist, K Hammerer, P Zoller, C Genes, M Ludwig, F Marquardt, P Treutlein, J Ye, and HJ Kimble. Single-atom cavity qed and optomechanics. *Physical Review A*, 81(2):023816, 2010.